

The Riemann Hypothesis Emerges in Dynamical Quantum Phase Transitions

ShiJie Wei,^{1,*} Yue Zhai,^{2,3,†} Quanfeng Lu,^{4,†} Wentao Yang,⁴ Pan Gao,¹ Chao Wei,^{3,2} Junda Song,^{3,2} Franco Nori,^{5,6} Tao Xin,^{3,‡} and Guilu Long^{4,7,1,§}

¹*Beijing Academy of Quantum Information Sciences, Beijing 100193, China*

²*Shenzhen Institute for Quantum Science and Engineering,*

Southern University of Science and Technology, Shenzhen 518055, China

³*International Quantum Academy, Futian District, Shenzhen, Guangdong 518048, China*

⁴*State Key Laboratory of Low-Dimensional Quantum Physics and
Department of Physics, Tsinghua University, Beijing 100084, China*

⁵*Center for Quantum Computing, RIKEN, Wakoshi, Saitama, 351-0198, Japan*

⁶*Quantum Research Institute, The University of Michigan, Ann Arbor, 48109-1040, MI, USA*

⁷*Tsinghua National Laboratory for Information Science and Technology, Beijing 100084, People's Republic of China*

The Riemann Hypothesis (RH), one of the most profound unsolved problems in mathematics, concerns the nontrivial zeros of the Riemann zeta function. Establishing connections between the RH and physical phenomena could offer new perspectives on its physical origin and verification. Here, we establish a direct correspondence between the nontrivial zeros of the zeta function and dynamical quantum phase transitions (DQPTs) in two realizable quantum systems, characterized by the averaged accumulated phase factor and the Loschmidt amplitude, respectively. This precise correspondence reveals that the RH can be viewed as the emergence of DQPTs at a specific temperature. We experimentally demonstrate this correspondence on a five-qubit spin-based system and further propose an universal quantum simulation framework for efficiently realizing both systems with polynomial resources, offering a quantum advantage for numerical verification of the RH. These findings uncover an intrinsic link between nonequilibrium critical dynamics and the RH, positioning quantum computing as a powerful platform for exploring one of mathematics' most enduring conjectures and beyond.

I. introduction

The Riemann zeta function is central to analytic number theory and has profound implications in mathematical physics. It admits a Dirichlet series representation valid for $\text{Re}(s) > 0, \text{Re}(s) \neq 1$:

$$\zeta(s) = \frac{1}{1 - 2^{1-s}} \sum_{n=1}^{\infty} \frac{(-1)^{n+1}}{n^s}. \quad (1)$$

The nontrivial zeros of the zeta function, conjectured by the celebrated Riemann Hypothesis (RH) to all lie on the critical line $\text{Re}(s) = \frac{1}{2}$, remain one of the most profound unsolved problems in mathematics. The RH underpins more than a thousand theorems in mathematics and forms the foundation of the modern RSA cryptographic system, for example, their distribution encodes the fine structure of prime numbers². Despite extensive numerical evidence^{3,4}, the RH remains unproven. Any new perspective on the zeta function is therefore of great significance, regardless of whether it ultimately leads to a proof or refutation of the RH.

Beyond its mathematical significance, the Riemann zeta function has long inspired deep physical analogies⁵, sparking the search for a possible physical origin of the

RH. The most influential idea in this direction is the Hilbert–Pólya conjecture^{6,7}, which suggests that the nontrivial zeros of the zeta function might correspond to the eigenvalues of an yet-unknown quantum Hamiltonian, motivating searches for such an operator^{8,9} and for signatures in diverse physical contexts, including relativistic amplitudes¹⁰, chaotic quantum scattering^{11,12}, quantum field theory¹³, and random matrix theory¹⁴. Significant progress^{15–17} has linked quantum systems to the Riemann zeta function through tailored state preparation, engineered spectra, and observable correspondences with its zeros. The search for a genuine physical realization, deeper connections and possible origins of the RH remains unknown.

Here, we propose a physical origin for the RH by demonstrating that the non-trivial zeros of the Riemann zeta function correspond directly to dynamical quantum phase transitions (DQPTs) in two distinct constructed quantum systems^{18–25}. Their physical realization starts with both models initialized in thermal equilibrium. We then drive them out of equilibrium by quenching with specific interaction Hamiltonians, which are engineered to imprint the zeta function's properties onto measurable observables. The average accumulated phase factor in the first system and the Loschmidt amplitude in the second both vanish at evolution times corresponding to the nontrivial zeros, revealing DQPTs. Furthermore, we introduce a quantum computational framework to efficiently simulate these dynamics on digital quantum computers, offering a clear quantum advantage for probing both DQPTs and the RH. This approach not only en-

* weisj@baqis.ac.cn; These authors contributed equally to this work.

† These authors contributed equally to this work.

‡ xintao@iqasz.cn

§ gllong@tsinghua.edu.cn

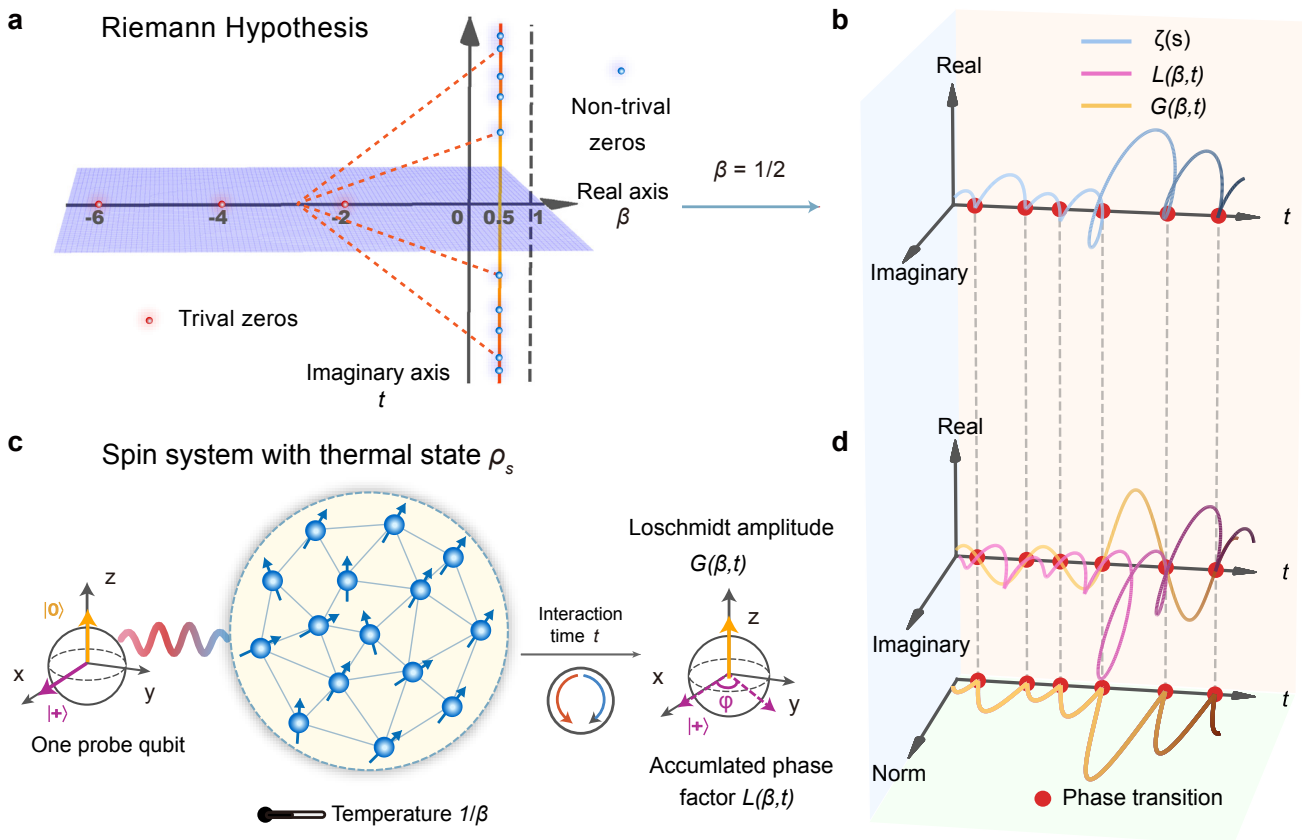


FIG. 1. **Correspondence between the Riemann zeta function and physical many-body systems.** **a** The RH in the complex plane (β, t) . It states that all nontrivial zeros of the zeta function lie on the critical line with real part $\beta = 1/2$. The distribution of the zeros of the zeta function is symmetric with respect to reflection across the real axis. **b** The zeta function $\zeta(1/2 + it)$ along the critical line. Each zero crossing, marked by a red dot, corresponds to a nontrivial Riemann zero. **c** Construction of two quantum systems, each consisting of a single probe spin coupled to a many-body system initialized in a thermal state at inverse temperature β . The composite system subsequently evolves under the system interactions with time-reversal symmetry. The blue arrow and red arrow represent the forward time evolution and backward evolution respectively. **d** The dynamics of the accumulated phase factor $\mathcal{L}(\beta, t)$ and the Loschmidt amplitude $\mathcal{G}(\beta, t)$ reproduce key features of the zeta function, exhibiting periodic vanishing-and-revival oscillations characteristics of DQPTs. The norms of both observables show correspondence with the norm of the zeta function.

ables the experimental observation of DQPTs tied to the zeros but also allows for the numerical exclusion of such critical behavior at non-zero points, thereby providing a physical pathway to investigate the RH.

As a proof of principle, we implement the first system experimentally on a five-qubit nuclear spin quantum processor. The measured coherence dynamics reproduce the oscillatory behavior of the zeta function and exhibit clear signatures of DQPTs aligned with its nontrivial zeros. For the second system, suitable for exploring higher-order zeros, large-scale numerical simulations confirm the correspondence up to the 10^{12} -th zero. Moreover, our gate-based framework constructs both models with polynomial resources and achieves at least a quadratic speedup over classical verification of RH zeros. These results establish a concrete bridge between number theory, quantum physics, and quantum technology, opening scalable pathways toward one of mathematics' most enduring mysteries and hinting at a deeper quantum structure underlying arithmetic.

II. Results

As shown in Fig. 1c, we study two distinct quantum dynamical processes, each initialized in a thermal state.

In both cases, a single probe qubit is coupled to the system, and the combined system evolves under an interaction Hamiltonian for a duration t . The average accumulated phase factor $\mathcal{L}(\beta, t)$ in the first setup directly encodes the behavior of $\zeta(s)$ in the thermodynamic limit, while the Loschmidt amplitude $\mathcal{G}(\beta, t)$ in the second captures the same feature in the joint thermodynamic and long-time limits. Remarkably, at $\beta = \frac{1}{2}$, both systems exhibit DQPTs, characterized by periodic vanishing-and-revival oscillations in the observables, which maps one-to-one to the nontrivial zeros. If the RH holds, such periodic revivals occur exclusively at this critical line $\beta = \frac{1}{2}$ in the first system. This correspondence indicates that RH can be explained as the DQPTs emerges only at inverse temperature $\beta = \frac{1}{2}$ in a specific quantum many body system. Moreover, the quantum systems exhibit

time-reversal symmetry, corresponding to the reflection symmetry of the zeta function. As summarized in Table I, we establish correspondence between the engineered quantum system and mathematical features of the zeta function. Together, these results establish a direct correspondence between the analytic features of the zeta function (Fig. 1b) and accessible quantum dynamics (Fig. 1d). We describe the construction of these quantum dynamics in the following sections.

TABLE I. **Correspondence between quantum systems and the Riemann zeta function.** Engineered quantum dynamics enable direct mapping of the zeta function, its non-trivial zeros, and its reflection symmetry.

Physical observables $\mathcal{L}(\beta, t)$ and $\mathcal{G}(\beta, t)$	Zeta function $\zeta(s)$
Accumulated phase factor $\mathcal{L}(\beta, t)$ vanishes at $\beta = 1/2$ as t increases	Zeros of $\zeta(s)$
Loschmidt amplitude $\mathcal{G}(\beta, t)$ vanishes at $\beta = 1/2$ as t increases	Zeros of $\zeta(s)$
DQPT occurs exclusively at $\beta = 1/2$	RH
Time-reversal invariance	Reflection symmetry of $\zeta(s)$

A. Probe Spin Coherence Signaling RH

We consider a quantum system with Hamiltonian $\mathcal{H}_0 = \sum_{n=1}^N E_n |n\rangle \langle n|$ and a logarithmic energy spectrum $E_n = \log n^{15}$. The system is initialized in the thermal equilibrium state $\rho_s = \frac{e^{-\beta \mathcal{H}_0}}{\mathcal{Z}(\beta, \mathcal{H}_0)}$, with partition function $\mathcal{Z}(\beta, \mathcal{H}_0) = \sum_{n=1}^N n^{-\beta}$. Constructing such a logarithmic energy spectrum is central to realizing the quantum system. Previous studies^{26,27} have typically employed analog simulation approaches, designing specific potential landscapes to approximate a logarithmic energy distribution. In our experiments, we prepare the corresponding thermal state directly by engineering level populations of density matrices in the nuclear spin quantum processor. More importantly, we present a universal quantum algorithm that prepares states and Hamiltonians with a logarithmic spectrum to arbitrary precision using only polynomial resources (see Sec. IID).

We define the average accumulated phase factor as $\mathcal{L}(\beta, t) = \text{Tr}[\rho_s e^{-i\mathcal{H}_0 t} \sigma_z^1]$, where $e^{-i\mathcal{H}_0 t} \sigma_z^1$ imprints a phase factor $(-1)^n e^{-iE_n t}$ on the n -th population of ρ_s . This yields

$$\begin{aligned} \mathcal{L}(\beta, t) &= \sum_{n=1}^N (-1)^n e^{-iE_n t} e^{-\beta E_n} / \mathcal{Z}(\beta, \mathcal{H}_0) \\ &= - \sum_{n=1}^N (-1)^{n+1} n^{-\beta-it} / \mathcal{Z}(\beta, \mathcal{H}_0). \end{aligned} \quad (2)$$

In the thermodynamic limit $N \rightarrow \infty$, $\mathcal{L}(\beta, t)$ is directly related to the zeta function $\zeta(\beta + it)$ as

$$\mathcal{Z}(\beta, \mathcal{H}_0) \mathcal{L}(\beta, t) \xrightarrow{N \rightarrow \infty} (2^{1-(\beta+it)} - 1) \zeta(\beta + it). \quad (3)$$

Hence, $\mathcal{L}(\beta, t)$ vanishes precisely when $\zeta(\beta+it)$ has a non-trivial zero. These zeros signal DQPTs in mixed states marked by non-analyticities in time²¹. We next establish a correspondence between these dynamical transitions and their equilibrium analogues.

Through the Choi–Jamiołkowski isomorphism, ρ_s can be mapped as $|\rho_s\rangle = \sum_{n=1}^N n^{-\beta/2} |n\rangle |n\rangle_a$, where $|n\rangle_a$ denotes an orthonormal basis in an ancillary Hilbert space isomorphic to the physical one. Under time evolution, the state evolves as $|\rho(t)\rangle = (e^{-i\mathcal{H}_0 t} \otimes \mathbb{I}_a) |\rho_s\rangle$, and the accumulated phase factor becomes $\mathcal{L}_p(\beta, t) = \langle \rho_s | e^{-i\mathcal{H}_0 t} \sigma_z^1 | \rho_s \rangle$. Consider an equilibrium system with boundary conditions imposed at two ends separated by a distance R , the boundary partition function in equilibrium statistical mechanics^{18,28} is given by

$$\mathcal{Z}_B(\beta, R, \mathcal{H}) = \langle \psi_a | e^{-R\mathcal{H}} | \psi_b \rangle, \quad (4)$$

where $|\psi_a\rangle = \frac{1}{C} \sum_{n=1}^N n^{-\beta/2} |n\rangle |n\rangle_a$ and $|\psi_b\rangle = \sigma_z^1 |\psi_a\rangle$ encode the boundary states and \mathcal{H} denotes the bulk Hamiltonian. By analytically continuing to complex time plane $R = it$, we obtain

$$\mathcal{Z}_B(\beta, it, \mathcal{H}_0 \otimes \mathbb{I}_a) = \langle \psi_a | e^{-i\mathcal{H}_0 t} \otimes \mathbb{I}_a | \psi_b \rangle = \mathcal{L}(\beta, t). \quad (5)$$

Thus, $\mathcal{L}(\beta, t)$ serves as a boundary partition function analytically continued to complex time. In the thermodynamic limit, the free-energy density is defined as^{19,29,30}

$$\begin{aligned} \mathcal{F}_1(\beta, t) &= - \lim_{N \rightarrow \infty} \frac{1}{\log N} \ln |\mathcal{Z}_B(\beta, it, \mathcal{H}_0 \otimes \mathbb{I}_a)| \\ &= - \lim_{N \rightarrow \infty} \frac{1}{\log N} \ln |\mathcal{L}(\beta, t)|. \end{aligned} \quad (6)$$

Singularities in $\mathcal{F}_1(\beta, t)$ occurs precisely at the nontrivial zeros, signaling the occurrence of DQPTs (see Methods IV B for a detailed derivation). If the RH holds, such singularities occur exclusively along the critical line $\beta = 1/2$, analogous to Lee–Yang zeros in thermal systems^{29–31}. For other temperatures $\beta \neq 1/2$, no such phenomenon arises.

According to equation (5), the same correspondence can be realized in a pure-state setting and we omit the detailed derivation here for brevity.

To render $\mathcal{L}(\beta, t)$ experimentally accessible, we introduce a probe spin initialized in the superposition state $|+\rangle = (|\uparrow\rangle + |\downarrow\rangle) / \sqrt{2}$. The probe is coupled to the system via $\mathcal{H}_{c1} = \lambda |\downarrow\rangle \langle \downarrow| \otimes \sigma_z^1$, where λ denotes the interaction strength. For an interaction time t_0 satisfying $\lambda t_0 = \pi$, this operation imprints a phase $(-1)^n$ on the n -th component of ρ_s . The joint system then evolves under the interaction Hamiltonian $\mathcal{H}_{c2} = |\downarrow\rangle \langle \downarrow| \otimes \mathcal{H}_0$ for a duration time t . The expectation value $\langle \sigma_x \rangle + i \langle \sigma_y \rangle$ of the probe spin directly yields $\mathcal{L}(\beta, t)$, providing experimental access to the dynamical signatures.

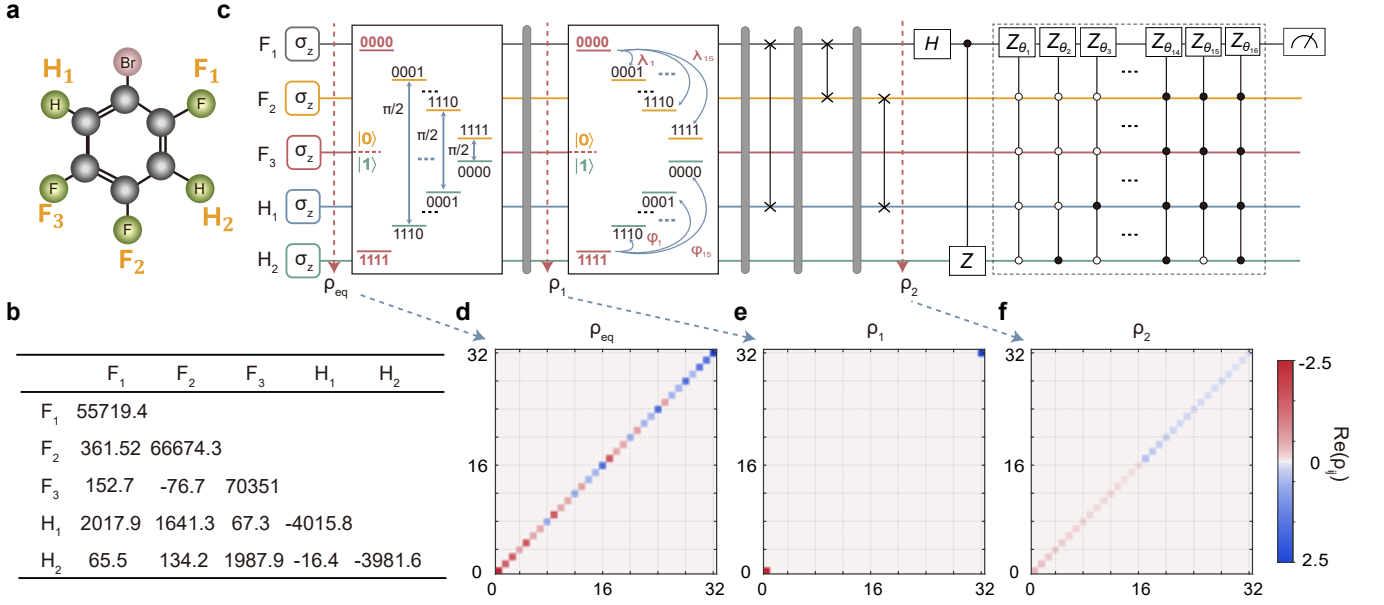


FIG. 2. **Physical system and quantum circuit for simulating the Riemann zeta function.** **a**, Molecular structure of the 1-bromo-2,4,5-trifluorobenzene. The five nuclear spins are encoded as qubits, with the F_1 spin serving as the probe qubit to extract the average accumulated phase factor. **b**, Measured Hamiltonian parameters. The chemical shifts ν_i are shown on the diagonal, while the off-diagonal elements represent the coupling strengths ($J_{ik} + 2D_{jk}$), both in units of Hz. **c**, Quantum circuit implementation, including thermal state preparation, controlled dynamical evolution, and coherence measurement. H denotes the Hadamard gate acting on the probe qubit. Coherent operations for state preparation and multi-qubit quantum gates are realized using shaped control pulses. The parameters λ_i and ψ_i for population transfer are determined by β , and the parameters θ_i are determined by t . **d**, **e**, **f**, Effective population evolution during state preparation. Here, we employ the traceless deviation density matrix to describe the state evolution.

B. Loschmidt echo corresponding to the RH

We further construct a concrete quantum system whose Loschmidt amplitude is directly linked to the zeta function, enabling the verification its large zeros. The system is initialized in the thermal equilibrium state ρ_s of the Hamiltonian \mathcal{H}_0 , and is coupled to a probe spin, forming the composite mixed state $\rho_0 = |\uparrow\rangle\langle\uparrow| \otimes \rho_s$. The joint system then evolves under the time-dependent Hamiltonian $\mathcal{H}_c = \sigma_x \otimes (\mathcal{H}_0 - \dot{\theta}(t)\mathcal{I})$ for $0 \leq t' \leq t$, with time-evolution operator $U(t') = \exp(-i \int_0^{t'} \mathcal{H}_c dt')$. Here $\theta(t') = \text{Im}(\log(\frac{1}{4} + \frac{it'}{2})) - \frac{t'}{2} \log \pi$ is the Riemann-Siegel theta function³², and its time derivative is $\dot{\theta}(t') = \frac{1}{2} \text{Re}(\psi(\frac{1}{4} + \frac{it'}{2})) - \frac{1}{2} \log \pi$, with ψ denoting the digamma function.

The generalized Loschmidt amplitude (GLA) is defined as the overlap of the initial density matrices with the time-evolution operator²¹. This yields

$$\begin{aligned} \mathcal{G}(\beta, t) &= \text{Tr}[e^{-i \int_0^t \mathcal{H}_c dt'} \rho_0] \\ &= \frac{1}{2\mathcal{Z}(\beta, \mathcal{H}_0)} (e^{i\theta(t)} \sum_{n=1}^N n^{-\beta-it} + e^{-i\theta(t)} \sum_{n=1}^N n^{-\beta+it}). \end{aligned} \quad (7)$$

For $N = \sqrt{t/2\pi}$, $\mathcal{G}(\frac{1}{2}, t)$ matches the Hardy Z-function $Z(t) = e^{i\theta t} \zeta(\frac{1}{2} + it)$, which admits a Riemann-Siegel ap-

proximation³²,

$$Z(t) = e^{i\theta(t)} \sum_{n=1}^N n^{-\frac{1}{2}-it} + e^{-i\theta(t)} \sum_{n=1}^N n^{-\frac{1}{2}+it} + \mathcal{O}(t^{-\frac{1}{4}}). \quad (8)$$

In the joint thermodynamic and long-time limit,

$$\mathcal{G}(\frac{1}{2}, t) \xrightarrow[N=\sqrt{t/2\pi}]{t \rightarrow \infty} \frac{e^{i\theta(t)} \zeta(\frac{1}{2} + it)}{2\mathcal{Z}(\frac{1}{2}, \mathcal{H}_0)}. \quad (9)$$

The modulus of the Loschmidt amplitude, $\mathcal{B}(t) = |\mathcal{G}(t)|^2$, defines the Loschmidt echo (LE), from which the Loschmidt rate (or dynamical free energy) is obtained as $\mathcal{F}_2(t) = -\lim_{N \rightarrow \infty} \frac{1}{\log N} \ln \mathcal{B}(t)$. Nonanalyticities in $\mathcal{F}_2(t)$ at critical times t_c , where $\mathcal{G}(\beta, t_c) = 0$, signal DQPTs^{19,21}. At $\beta = \frac{1}{2}$, the LE exhibits a vanishing-and-revival dynamic, vanishing at the critical times t_c that correspond to the nontrivial Riemann zeros. As the evolution time t increases, this correspondence becomes increasingly accurate.

We demonstrate that the GLA can be accessed via the expectation value of σ_z on the probe spin (see Methods IV C). Extended Data Fig. 1a shows numerical simulations of a three-spin system reproducing the zeros of the GLA corresponding to nontrivial Riemann zeros with imaginary parts in the range $[420, 450]$. Extending to a ten-spin system enables access to zeros with imaginary parts in $[6.595 \times 10^6, 6.595 \times 10^6 + 10]$, corresponding to the 13,502,344-th to 13,502,366-th zeros, as shown in Extended Data Fig. 1b. An eighteen-spin system further

captures the DQPTs linked to the 10^{12} -th and nearby zeros as shown in Extended Data Fig. 1c. Notably, the deviation between the estimated zeros and exact zeros decreases with increasing t , indicating improved precision of correspondence at larger Riemann zeros. In addition, we consider a pure initial state $\frac{1}{C} \sum_{n=1}^N n^{-\beta/2} |0\rangle|n\rangle$ evolving under the system Hamiltonian \mathcal{H}_c . This system likewise exhibits DQPTs, characterized by nonanalytic behavior in the Loschmidt amplitude, whose zeros correspond to the nontrivial zeros of the zeta function.

C. Experimental verification using nuclear spins

The connection between physical quantum systems and the RH offers a novel method for experimentally probing the behavior of the zeta function through controlled Hamiltonian dynamics. As a proof-of-principle demonstration, we realized a five-qubit system on a nuclear magnetic resonance (NMR) platform. The qubits are encoded in the nuclear spins of a 1-bromo-2,4,5-trifluorobenzene molecule, partially aligned in the nematic liquid crystal solvent N-(4-methoxybenzaldehyde)-4-butylaniline (MBBA)^{33–35}. The molecule consists of three ^{19}F nuclei and two ^1H nuclei. A single nuclear spin serves as the probe qubit, with the remaining spins constituting a sixteen-dimensional working system. The effective Hamiltonian of this five-qubit system in the rotating frame is given by

$$\mathcal{H}_{\text{NMR}} = \sum_{j=0}^4 \pi \nu_j \frac{\sigma_z^j}{2} + \sum_{j < k} \frac{\pi}{2} (J_{jk} + 2D_{jk}) \sigma_z^j \sigma_z^k, \quad (10)$$

where σ_z^j is the Pauli- z operator on the j -th spin, ν_j denotes the chemical shift of the j -th spin, and $(J_{jk} + 2D_{jk})$ represents the effective coupling strength between spins j and k . Here, J_{jk} and D_{jk} correspond to the scalar and residual dipolar couplings, respectively. The molecular structure and Hamiltonian parameters are illustrated in Figs. 2a and 2b, respectively. All experiments were implemented on a Bruker Avance III 600 MHz spectrometer at $T = 305$ K.

There are two major challenges in experimentally realizing this constructed Hamiltonian dynamics. The first is the preparation of thermal states, and the second is the implementation of controlled dynamical evolution. NMR systems are ensemble-based and naturally begin in a thermal equilibrium state $\rho_{\text{eq}} \sim \gamma_{\text{F}} \sum_{i=1}^3 \sigma_z^i + \gamma_{\text{H}} \sum_{i=4}^5 \sigma_z^i$, after ignoring the identity component for convenience, where γ_{F} and γ_{H} denote the gyromagnetic ratios of the fluorine and hydrogen nuclei, respectively. Starting from the initial state ρ_{eq} , we can redistribute the level populations via coherent control and subsequently eliminate the off-diagonal elements to arrive at a state close to the target $\rho_0(\beta) \sim \sigma_z \otimes \sum_{n=1}^{16} n^{-\beta} |n\rangle\langle n|$.

As shown in Fig. 2c, our procedure for preparing the thermal state primarily consists of the following steps. (i) Elimination of populations on all levels except the

$|\uparrow\uparrow\uparrow\uparrow\rangle$ and $|\downarrow\downarrow\downarrow\downarrow\rangle$ levels. By exploiting the antisymmetric population distribution between pairs of energy levels in ρ_{eq} , we apply selective $\pi/2$ rotations to each such pair, excluding the states $|\uparrow\uparrow\uparrow\uparrow\rangle$ and $|\downarrow\downarrow\downarrow\downarrow\rangle$, to convert the diagonal population matrix into a purely off-diagonal form. Subsequently, a gradient field along the z -direction is applied to decohere these off-diagonal elements. (ii) Transfer of population from $|\uparrow\uparrow\uparrow\uparrow\rangle$ and $|\downarrow\downarrow\downarrow\downarrow\rangle$ to other levels, according to the target distribution encoded in $\rho_0(\beta)$. This is achieved by implementing coherent $R_y(\lambda)$ [or $R_y(\psi)$] rotations between $|\uparrow\uparrow\uparrow\uparrow\rangle$ (or $|\downarrow\downarrow\downarrow\downarrow\rangle$) and other levels within the $|\uparrow\rangle$ [or $|\downarrow\rangle$] subspace of the probe qubit. The rotation angles are determined by β . During this process, the off-diagonal terms generated are also eliminated by applying a gradient pulse. However, since the gradient field alone cannot fully suppress coherence within homonuclear subspaces. SWAP operations are applied between the F and H spin subspaces in conjunction with the gradient field to ensure complete decoherence. Finally, the desired thermal state is prepared. Further details can be found in the Methods.

As outlined in Section II A, two controlled Hamiltonian dynamics under \mathcal{H}_{c1} and \mathcal{H}_{c2} are to be implemented. The first $e^{-i\mathcal{H}_{c1}\pi/\lambda}$ corresponds to a controlled- Z gate between the probe spin and last spin. The second $e^{-i\mathcal{H}_{c2}t}$ can be decomposed into multiple multi-qubit controlled- $R_z(\theta_n)$ operations. The rotation angles are given by $\theta_n = t \log n$, where t denotes the imaginary part of the RH complex plane. Last, we measure the coherence $\mathcal{L}(\beta, t) = \langle \uparrow | \rho_f | \downarrow \rangle$ of the probe spin on the final state $\rho_f = U_{\text{tot}} \rho_0 U_{\text{tot}}^\dagger$ where $U_{\text{tot}} = e^{-i\mathcal{H}_{c2}t} e^{-i\mathcal{H}_{c1}\pi/\lambda} (H \otimes I)$. Figure 2 illustrates the full experimental sequence, from initial state preparation to final measurement. To enhance control accuracy, we implement all coherent operations and unitary evolutions using shaped pulses optimized via a gradient ascent pulse technique³⁶, yielding a numerical simulation fidelity exceeding 99.5%.

We conducted three types of experiments to comprehensively validate the theoretical predictions. First, we prepare the thermal state $\rho_0(\beta)$ with $\beta = 0.5$ (corresponding to the RH) and vary the evolution time t under the Hamiltonian \mathcal{H}_{c2} . Second, we prepare another thermal state $\rho_0(\beta)$ with $\beta = 0.3$, which lies off the critical line of the RH, we again vary the evolution time t . Third, we fix the evolution time at $t = 14.13$, corresponding to the imaginary part of the first nontrivial Riemann zero, and scan β over the range $[0.1, 0.9]$. Then the coherence dynamics $\mathcal{L}(\beta, t)$ of the probe qubit is measured in each configuration. Figures 3a and 3b present the coherence dynamics $\mathcal{L}(\beta, t)$ under different values of β . When $\beta = 0.5$, the coherence of the probe spin exhibits recurring vanishing-and-revival behavior, and the points where both the real and imaginary parts of $\mathcal{L}(\beta, t)$ approach zero correspond to Riemann zeros. As a demonstration, $t_1 = 14.12$ ($t_1^{\text{th}} = 14.13$), $t_2 = 20.96$ ($t_2^{\text{th}} = 21.02$), $t_3 = 25.09$ ($t_3^{\text{th}} = 25.01$), $t_4 = 30.44$ ($t_4^{\text{th}} = 30.43$), and $t_5 = 32.93$ ($t_5^{\text{th}} = 32.94$) coherence zeros are extracted through polynomial fitting of the experimental

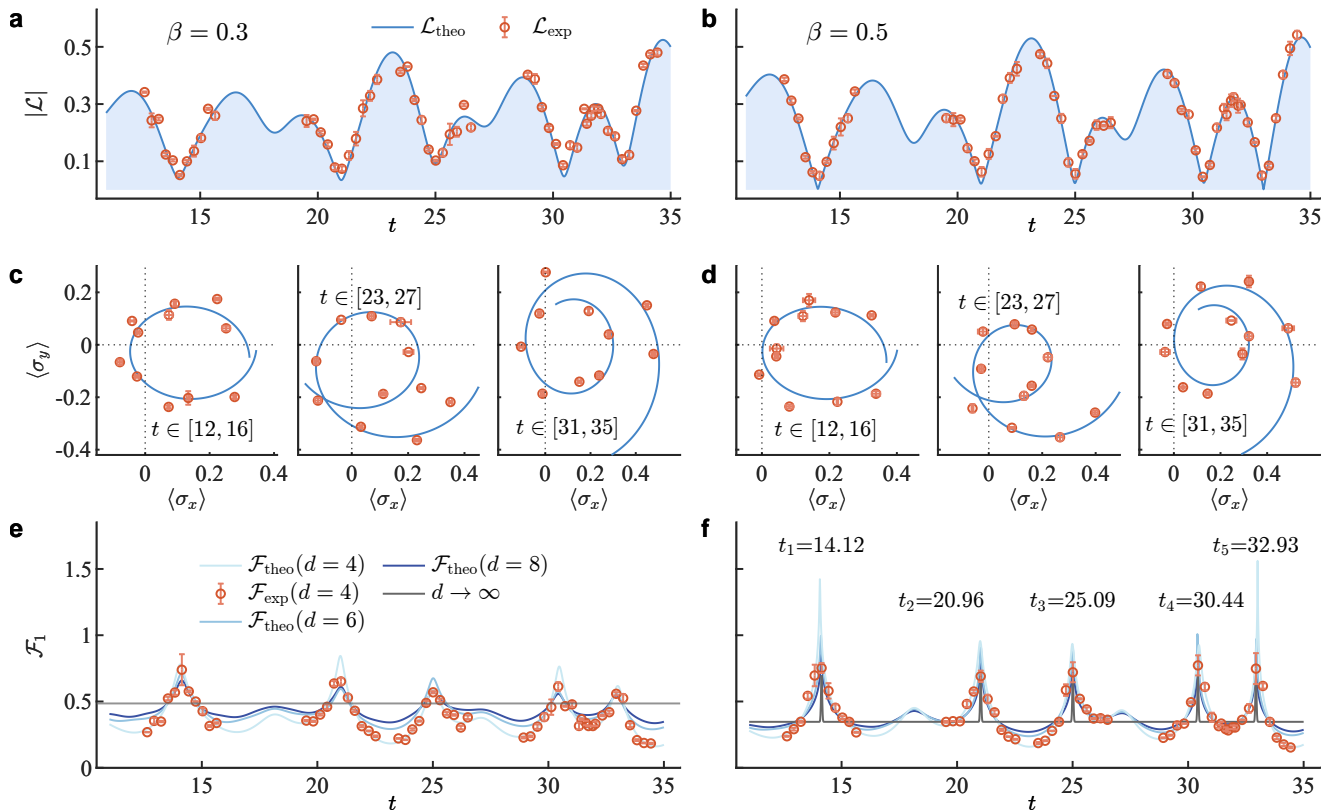


FIG. 3. **The coherence dynamics $\mathcal{L}(\beta, t)$ of the probe qubit and the non-trivial Riemann zeros.** **a**, Measured probe spin coherence $\mathcal{L}(0.3, t)$ versus evolution time t . **b**, $\mathcal{L}(0.5, t)$ versus time t for $\beta = 0.5$. Solid lines represent numerically calculated values of the probe spin coherence. **c**, **d**, The first, third, and fifth Riemann zeros identified from the zeros of the probe spin coherence, where both the real part $\langle \sigma_x \rangle$ and the imaginary part $\langle \sigma_y \rangle$ simultaneously vanish. **e**, **f**, The corresponding free-energy density computed using Eq. (6). $d = \log N$ reflects the system's effective number of degrees of freedom. Theoretically predicted Riemann zeros are indicated by the values on the horizontal line for comparison. For $\beta = 0.5$, which corresponds to the critical line of the RH, the dynamics of the probe spin coherence exhibit multiple zeros, each matching one-to-one with Riemann zeros. In contrast, for $\beta = 0.3$, which lies outside the RH, no zeros are observed in the spin coherence dynamics. Here and elsewhere, error bars represent 1σ confidence intervals coming from the repeated experiments. These findings establish our approach as a powerful tool for investigating the RH and its zeros within a controlled quantum many-body system.

data. These values agree well with the ideal zeros of the zeta function. In contrast, for $\beta = 0.3$, the coherence dynamics show no discernible vanishing-and-revival behavior, and no significant coherence zeros are observed. Figure 4 shows the behavior of the coherence as a function of β . The results clearly indicate the emergence of coherence zeros and DQPTs when crossing the critical line $\beta = 0.5$, in accordance with the RH.

D. Simulating the RH within a universal quantum computing framework

Since the two quantum systems introduced above are strongly correlated, their direct realization on a gate-based quantum computer is highly nontrivial³⁷. Therefore, we propose an efficient computational framework that enables their realization on a universal gate-based quantum computer. The constructions in Sections II A

and II B can be reduced to two fundamental tasks:

- (i) Preparation of the initial thermal state, which encodes the real part of the zeta argument.
- (ii) Simulation of time evolution under the target Hamiltonian, which encodes the imaginary part.

The initial state $|\psi_0\rangle = \frac{1}{\mathcal{C}} \sum_{n=1}^N n^{-\beta/2} |n\rangle$ can be prepared to precision ε with success possibility at least $(\frac{1}{2} - \frac{\varepsilon}{3})$ using polynomial qubits and basic gates. We further show that the evolution $U(t) = e^{-i\mathcal{H}_0 t}$ for $\mathcal{H}_0 = \sum_{n=1}^N \log n |n\rangle \langle n|$ can be also implemented to precision ξ with polynomial resources, and controlled evolutions incur the same polynomial overhead. These guarantees ensure scalability of our method on a gate-based quantum computer (see Methods IV D for details).

We then apply this framework to accelerate the verification and probing of nontrivial zeros via the Riemann-Siegel formula, which decomposes the zeta function into two partial summations that can be

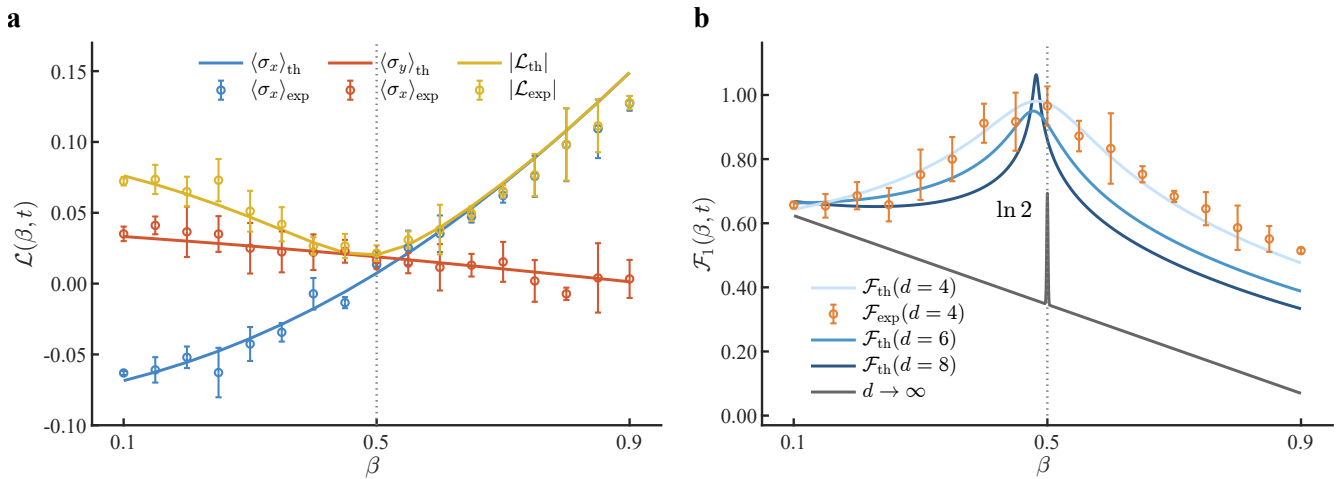


FIG. 4. **The coherence dynamics $\mathcal{L}(\beta, t)$ of the probe qubit and the free energy density $\mathcal{F}_1(\beta, t)$ of the quantum system varying with the value of β .** The evolution time t is set to 14.13, the imaginary part of the first RH zero. **a**, As β passes through the point associated with the RH, the coherence approximately drops to zero, with its non-vanishing value being a consequence of finite-size effects. **b**, Non-analytic behavior of the free energy density as β passes through the point associated with the RH. In the thermodynamic limit $d \rightarrow \infty$, the free-energy density undergoes a sudden change from $(1 - \beta) \ln 2$ to $\ln 2$ at $\beta = 1/2$, signaling the occurrence of DQPTs.

evaluated using systems similar to that in Section II A. To achieve a total error δ in the zeta function, the quantum circuit complexities are bounded by $\text{Poly}(\log \delta^{-1}, \log |t|, \log(1 - \beta)^{-1}, \log \beta^{-1})$, while the corresponding sample complexities are bounded by $\mathcal{O}(\delta^{-1})(1 - \beta)^{-1}|t|^{(1-\beta)/2}$ and $\mathcal{O}(\delta^{-1})\beta^{-1}|t|^{(1-\beta)/2}$, respectively. Hence the overall computational complexity (See Methods IV E for details) is bounded by:

$$\delta^{-1}|t|^{(1-\beta)/2}\text{Poly}(\log \delta^{-1}, \log |t|, (1 - \beta)^{-1}, \beta^{-1}). \quad (11)$$

Specializing to locating and verifying nontrivial zeros, where $\frac{1}{2} \leq \beta \leq 1 - \frac{1}{\mathcal{O}((\log |t|)^{2/3}(\log \log |t|)^{1/3})}$ ³⁸, this simplifies to

$$\delta^{-1}|t|^{(1-\beta)/2}\text{Poly}(\log \delta^{-1}, \log |t|). \quad (12)$$

Thus the $|t|$ -dependence reduces from $\sqrt{|t|}$ (direct Riemann–Siegel evaluation) to $|t|^{(1-\beta)/2}$ (at most $|t|^{1/4}$), yielding at least a quadratic speedup. Extended Data Table 1 summarizes these complexity bounds.

III. Discussion

In this work, we have established a direct correspondence between the RH and the dynamics of quantum many-body systems, and experimentally verified this connection on a physical platform. The mapping between nontrivial Riemann zeros and DQPTs reveals a deep and unexplored bridge between number theory and quantum physics. In particular, we have demonstrated that a thermally equilibrated quantum system, when driven by a tailored Hamiltonian, undergoes time-domain phase transitions whose critical points align precisely with the Riemann zeros. To verify large Riemann zeros, we also construct a quantum system which undergoes time-domain phase transitions whose critical points align in-

creasingly accurately to the large Riemann zeros. Together, these results suggest that the mysterious structure of the zeta function may admit a physical interpretation in terms of quantum critical dynamics.

Importantly, we demonstrated that both classes of systems considered here can be constructed on a universal quantum computer in polynomial time and numerical verification of the RH can be achieved by our method with at least a quadratic speedup over classical methods. Beyond this, our results suggest that Riemann zeros also encode signatures of information propagation in quantum systems, motivating future studies of their relationship to out-of-time-ordered correlators (OTOCs)^{39–41} and other diagnostics of quantum chaos.

Given the inherent difficulty of verifying the RH using classical computation, our approach opens a path toward leveraging quantum computing as an algorithmic tool for probing one of mathematics’ most enduring open problems. We note that more efficient classical methods for evaluating the Riemann zeta function on the critical line $\beta = \frac{1}{2}$ are known^{3,42}. Our ongoing work explores how the proposed framework can accelerate the most time-consuming subroutines of these methods, thereby further improving their overall efficiency. Moreover, the framework presented here can be extended to the evaluation of other series and special functions, potentially defining a broader class of number-theoretic benchmarks for demonstrating quantum advantage. For example, the prime number distribution can be constructed using the Riemann function, thus allowing this computational framework to be further applied to the calculation of Witten index in string theory and supersymmetry theory.

1. M. S. Milgram, Integral and Series Representations of Riemann's Zeta Function and Dirichlet's Eta Function and a Medley of Related Results, *J. Math.* **2013**, 181724 (2013).
2. H. Bui, Large gaps between consecutive zeros of the Riemann zeta-function, *J. Number Theory* **131**, 67 (2011).
3. A. M. Odlyzko, The 10^{22} -nd zero of the Riemann zeta function, *Contemp. Math.* **290**, 139 (2001).
4. J. W. Bober and G. A. Hiary, New Computations of the Riemann Zeta Function on the Critical Line, *Exp. Math.* **27**, 125 (2018).
5. D. Schumayer and D. A. Hutchinson, Colloquium: Physics of the Riemann hypothesis, *Rev. Mod. Phys.* **83**, 307 (2011).
6. M. V. Berry, Riemann's zeta function: A model for quantum chaos?, in *Quantum Chaos and Statistical Nuclear Physics: Proceedings of the 2nd International Conference on Quantum Chaos and the 4th International Colloquium on Statistical Nuclear Physics, Held at Cuernavaca, Mexico, January 6–10, 1986* (Springer, 2005) pp. 1–17.
7. M. V. Berry and J. P. Keating, A new asymptotic representation for $\zeta(1/2 + it)$ and quantum spectral determinants, *Proc. R. Soc. Lond., Ser. A* **437**, 151 (1992).
8. M. Srednicki, Nonclassical degrees of freedom in the Riemann Hamiltonian, *Phys. Rev. Lett.* **107**, 100201 (2011).
9. C. M. Bender, D. C. Brody, and M. P. Müller, Hamiltonian for the zeros of the Riemann zeta function, *Phys. Rev. Lett.* **118**, 130201 (2017).
10. G. N. Remmen, Amplitudes and the Riemann Zeta function, *Phys. Rev. Lett.* **127**, 241602 (2021).
11. M. C. Gutzwiller, Stochastic behavior in quantum scattering, *Phys. D (Amsterdam, Neth.)* **7**, 341 (1983).
12. R. Bhaduri, A. Khare, and J. Law, Phase of the Riemann ζ function and the inverted harmonic oscillator, *Phys. Rev. E* **52**, 486 (1995).
13. D. Spector, Supersymmetry and the Möbius inversion function, *Commun. Math. Phys.* **127**, 239 (1990).
14. C. P. Hughes, J. P. Keating, and N. 'Connell, Random matrix theory and the derivative of the Riemann zeta function, *Proc. R. Soc. Lond., Ser. A* **456**, 2611 (2000).
15. R. Mack, J. P. Dahl, H. Moya-Cessa, W. T. Strunz, R. Walser, and W. P. Schleich, Riemann ζ function from wave-packet dynamics, *Phys. Rev. A* **82**, 032119 (2010).
16. C. Feiler and W. P. Schleich, Entanglement and analytical continuation: an intimate relation told by the Riemann zeta function, *New J. Phys.* **15**, 063009 (2013).
17. C. Feiler and W. P. Schleich, Dirichlet series as interfering probability amplitudes for quantum measurements, *New J. Phys.* **17**, 063040 (2015).
18. M. Heyl, Dynamical quantum phase transitions: a review, *Rep. Progr. Phys.* **81**, 054001 (2018).
19. M. Heyl, A. Polkovnikov, and S. Kehrein, Dynamical quantum phase transitions in the transverse-field Ising model, *Phys. Rev. Lett.* **110**, 135704 (2013).
20. C. Karrasch and D. Schuricht, Dynamical phase transitions after quenches in nonintegrable models, *Phys. Rev. B* **87**, 195104 (2013).
21. M. Heyl and J. Budich, Dynamical topological quantum phase transitions for mixed states, *Phys. Rev. B* **96**, 180304 (2017).
22. U. Bhattacharya, S. Bandyopadhyay, and A. Dutta, Mixed state dynamical quantum phase transitions, *Phys. Rev. B* **96**, 180303 (2017).
23. H. Lang, Y. Chen, Q. Hong, and H. Fan, Dynamical quantum phase transition for mixed states in open systems, *Phys. Rev. B* **98**, 134310 (2018).
24. J. A. Muniz, D. Barberena, R. J. Lewis-Swan, D. J. Young, J. R. Cline, A. M. Rey, and J. K. Thompson, Exploring dynamical phase transitions with cold atoms in an optical cavity, *Nature* **580**, 602 (2020).
25. L. Zhou, Q.-h. Wang, H. Wang, and J. Gong, Dynamical quantum phase transitions in non-Hermitian lattices, *Phys. Rev. A* **98**, 022129 (2018).
26. F. Gleisberg, R. Mack, K. Vogel, and W. P. Schleich, Factorization with a logarithmic energy spectrum, *New J. Phys.* **15**, 023037 (2013).
27. D. Cassettari, G. Mussardo, and A. Trombettoni, Holographic realization of the prime number quantum potential, *PNAS* **2**, pgac279 (2023).
28. A. LeClair, G. Mussardo, H. Saleur, and S. Skorik, Boundary energy and boundary states in integrable quantum field theories, *Nucl. Phys. B* **453**, 581 (1995).
29. X. Peng, H. Zhou, B.-B. Wei, J. Cui, J. Du, and R.-B. Liu, Experimental observation of Lee-Yang zeros, *Phys. Rev. Lett.* **114**, 010601 (2015).
30. A. Francis, D. Zhu, C. Huerta Alderete, S. Johri, X. Xiao, J. K. Freericks, C. Monroe, N. M. Linke, and A. F. Kemper, Many-body thermodynamics on quantum computers via partition function zeros, *Sci. Adv.* **7**, eabf2447 (2021).
31. B.-B. Wei and R.-B. Liu, Lee-Yang zeros and critical times in decoherence of a probe spin coupled to a bath, *Phys. Rev. Lett.* **109**, 185701 (2012).
32. J. de Reyna, High precision computation of Riemann's zeta function by the Riemann-Siegel formula, I, *Math. Comput.* **80**, 995 (2011).
33. R. Shankar, S. S. Hegde, and T. Mahesh, Quantum simulations of a particle in one-dimensional potentials using NMR, *Phys. Lett. A* **378**, 10 (2014).
34. Z. Luo, J. Li, Z. Li, L.-Y. Hung, Y. Wan, X. Peng, and J. Du, Experimentally probing topological order and its breakdown through modular matrices, *Nat. Phys.* **14**, 160 (2018).
35. X. Nie, X. Zhu, Y.-a. Fan, X. Long, H. Liu, K. Huang, C. Xi, L. Che, Y. Zheng, Y. Feng, *et al.*, Self-Consistent Determination of Single-Impurity Anderson Model Using Hybrid Quantum-Classical Approach on a Spin Quantum Simulator, *Phys. Rev. Lett.* **133**, 140602 (2024).
36. N. Khaneja, T. Reiss, C. Kehlet, T. Schulte-Herbrüggen, and S. J. Glaser, Optimal control of coupled spin dynamics: design of NMR pulse sequences by gradient ascent algorithms, *J. Magn. Reson.* **172**, 296 (2005).
37. C.-F. Chen, M. Kastoryano, F. G. S. L. Brandão, and A. Gilyén, Efficient quantum thermal simulation, *Nature* **646**, 561 (2025).
38. M. J. Mossinghoff, T. S. Trudgian, and A. Yang, Explicit zero-free regions for the Riemann zeta-function, *Res. Number Theory* **10**, 11 (2024).
39. M. Gärttner, J. G. Bohnet, A. Safavi-Naini, M. L. Wall, J. J. Bollinger, and A. M. Rey, Measuring out-of-time-order correlations and multiple quantum spectra in a trapped-ion quantum magnet, *Nat. Phys.* **13**, 781 (2017).
40. J. Braumüller, A. H. Karamlou, Y. Yanay, B. Kannan, D. Kim, M. Kjaergaard, A. Melville, B. M. Niedzielski, Y. Sung, A. Vepsäläinen, *et al.*, Probing quantum information propagation with out-of-time-ordered correlators, *Nat. Phys.* **18**, 172 (2022).
41. Google Quantum AI and Collaborators, Observation of constructive interference at the edge of quantum ergodicity, *Nature* **646**, 825 (2025).

42. G. A. Hiary, Fast methods to compute the Riemann zeta function, *Annals of Math.* , 891 (2011).
43. L. Grover and T. Rudolph, Creating superpositions that correspond to efficiently integrable probability distributions, [arXiv preprint quant-ph/0208112](#) (2002).
44. G.-L. Long and Y. Sun, Efficient scheme for initializing a quantum register with an arbitrary superposed state, *Phys. Rev. A* **64**, 014303 (2001).
45. P. Borwein, An efficient algorithm for the Riemann zeta function, in *Canadian Mathematical Society Conference Proceedings*, Vol. 27 (2000) pp. 29–34.
46. D. Litinski, Quantum schoolbook multiplication with fewer Toffoli gates, [arXiv preprint arXiv:2410.00899](#) (2024).
47. S. Akiyama and Y. Tanigawa, Multiple zeta values at non-positive integers, *The Ramanujan Journal* **5**, 327 (2001).

IV. Methods

A. Thermal state preparation in experiment

The preparation sequence, shown in the main text, consists of two analytically designed line-selective shaped pulses, four pulsed field gradients, and three SWAP gates. The first shaped pulse selectively depletes population from all states except $|\uparrow\uparrow\uparrow\uparrow\rangle$ and $|\downarrow\downarrow\downarrow\downarrow\rangle$, which serve as logical sources for encoding the thermal-equivalent distribution. A gradient pulse is applied immediately afterward to suppress non-diagonal coherence terms generated in this step. The second shaped pulse redistributes the populations from $|\uparrow\uparrow\uparrow\uparrow\rangle$ and $|\downarrow\downarrow\downarrow\downarrow\rangle$ into a target position matching the desired thermal distribution. This step introduces zeroth-order coherences that cannot be fully removed by gradients alone. To address this, three SWAP operations are inserted before the final two gradient pulses, transferring coherence terms from homonuclear fluorine spins to heteronuclear channels, where they can be completely dephased. Below, we detail the function of each component in the preparation protocol.

The thermal equilibrium state of this five-qubit system is highly mixed. It can be described by a deviation density matrix of the form:

$$\rho_{\text{eq}} \propto \gamma_F(\sigma_z^1 + \sigma_z^2 + \sigma_z^3) + \gamma_H(\sigma_z^4 + \sigma_z^5), \quad (13)$$

where γ_H and γ_F are the gyromagnetic ratios for ^1H and ^{19}F nuclei, and σ_z^i is the Pauli-Z operator for the i -th qubit. This matrix is traceless and diagonal, with the maximal populations residing in the $|\uparrow\uparrow\uparrow\uparrow\rangle$ and $|\downarrow\downarrow\downarrow\downarrow\rangle$ states. Furthermore, pairs of symmetric basis states (e.g., $|\uparrow\uparrow\uparrow\downarrow\rangle$ and $|\downarrow\downarrow\downarrow\uparrow\rangle$) possess populations of equal magnitude but opposite sign, satisfying $P_{|\uparrow\uparrow\uparrow\downarrow\rangle} + P_{|\downarrow\downarrow\downarrow\uparrow\rangle} = 0$. This intrinsic symmetry is key to our line-selective approach, allowing us to manipulate populations.

The first shaped pulse is designed to selectively deplete the population of all energy levels except for the $|\uparrow\uparrow\uparrow\uparrow\rangle$ and $|\downarrow\downarrow\downarrow\downarrow\rangle$ states, which serve as the source states for subsequent redistribution. This is achieved by applying a series of analytically constructed $\pi/2$ line-selective rotations between all pairs of symmetric basis states (e.g., $|\uparrow\uparrow\uparrow\downarrow\rangle$ and $|\downarrow\downarrow\downarrow\uparrow\rangle$). For a given pair of states, say $|x\rangle$ and $|\bar{x}\rangle$, their initial populations are represented by a diagonal matrix $\begin{bmatrix} a & 0 \\ 0 & -a \end{bmatrix}$. Applying an $R_y(\pi/2)$ rotation transforms this to $\begin{bmatrix} 0 & a \\ a & 0 \end{bmatrix}$. Since these pairs have opposite initial populations in ρ_{eq} , applying a $\pi/2$ rotation along the y -axis effectively converts the diagonal population matrix to a purely off-diagonal one, which is then removed by a subsequent gradient pulse along the z -direction. Because the system has an odd number of qubits, this procedure avoids generating zeroth-order coherences. A pulsed field gradient is then applied to remove any residual higher-order coherences, leading to a diagonal intermediate state ρ_1 in which only the $|\uparrow\uparrow\uparrow\uparrow\rangle$ and $|\downarrow\downarrow\downarrow\downarrow\rangle$ populations remain.

The second shaped pulse redistributes the populations of $|\uparrow\uparrow\uparrow\uparrow\rangle$ and $|\downarrow\downarrow\downarrow\downarrow\rangle$ into a coherent superposition that encodes the target thermal-equivalent state. This state is represented by:

$$\rho = \sigma_z \otimes \sum_{n=1}^{16} \frac{n^{-\beta}}{\mathcal{N}^2} |n\rangle\langle n|, \quad (14)$$

with the normalization constant \mathcal{N} . This is accomplished by a sequence of analytically determined line-selective rotations that couple the source basis to the remaining basis. Each rotation is precisely calculated to transfer a fraction of the population from $|\uparrow\uparrow\uparrow\uparrow\rangle$ or $|\downarrow\downarrow\downarrow\downarrow\rangle$ to a selected target basis. The rotation angles are derived from $\theta_k = 2 \sin^{-1} \left(\sqrt{p_k/P_{\text{rem}}} \right)$, where p_k is the target population of the k -th basis and P_{rem} is the remaining unallocated population. This asymmetric redistribution process inevitably introduces zeroth-order coherences, particularly among homonuclear fluorine spins, which cannot be effectively suppressed by gradient fields alone.

To address the issue of residual homonuclear coherences, we employ a SWAP-assisted gradient scheme. The core idea is to transfer these coherences from homonuclear channels to heteronuclear ones, where they can be completely dephased by a gradient pulse. The sequence begins with a SWAP(1,4) gate to exchange the states of qubit 1 (^{19}F) and qubit 4 (^1H). This operation converts fluorine-fluorine coherences (e.g., between qubits 1 and 2) into heteronuclear coherences that can be dephased by the first gradient pulse. A second SWAP(1,4) gate restores the original logical labeling. To eliminate the remaining fluorine-fluorine coherence between qubits 2 and 3, we next apply a SWAP(2,4) gate, shifting this coherence to the heteronuclear (3,4) channel, which is then removed by the second gradient pulse. For increased efficiency, the two middle SWAP gates, SWAP(1,4) and SWAP(2,4), can be combined into a single SWAP(1,2) operation. A final SWAP(2,4) then returns the system to its original qubit configuration. This sequence of SWAP gates and gradient pulses ensures that all zeroth-order coherences are effectively eliminated, yielding a clean thermal-equivalent state with a numerical fidelity exceeding 99%.

B. Non-analytic behavior of the free energy

The free energy density is defined as

$$\mathcal{F}_1(\beta, t) = \lim_{N \rightarrow \infty} -\frac{1}{d} \ln |\mathcal{L}(\beta, t)|, \quad (15)$$

where $d = \log N$ denotes the number of degrees of freedom. According to Eq. (2), the accumulated phase factor can be expressed as

$$\mathcal{L}(\beta, t) = S_N(s)/\mathcal{Z}(\beta, \mathcal{H}_0), \quad (16)$$

where $S_N(s) = -\sum_{n=1}^N (-1)^{n+1} n^{-s}$. We prove that (see Supplementary Notes 1 and 2):

$$\lim_{N \rightarrow \infty} -\frac{1}{d} \ln(|S_N(s)|) = \begin{cases} \beta \ln 2, & \text{Riemann zeros,} \\ 0, & \text{Otherwise,} \end{cases} \quad (17)$$

and

$$\lim_{N \rightarrow \infty} -\frac{1}{d} \ln(\mathcal{Z}(\beta, \mathcal{H}_0)) = \begin{cases} (\beta - 1) \ln 2, & 0 < \beta < 1, \\ 0, & \beta > 1. \end{cases} \quad (18)$$

Combining these results, the free energy density in the thermodynamic limit is given by

$$\begin{aligned} & \mathcal{F}_1(\beta, t) \\ &= \lim_{N \rightarrow \infty} -\frac{1}{d} \left(\ln(|S_N(s)|) - \ln(\mathcal{Z}(\beta, \mathcal{H}_0)) \right) \\ &= \begin{cases} \ln 2, & \text{Riemann zeros,} \\ (1 - \beta) \ln 2, & 0 < \beta < 1, \notin \text{Riemann zeros,} \\ 0, & \beta > 1. \end{cases} \quad (19) \end{aligned}$$

This result demonstrates that the free energy density exhibits a non-analytic divergence at the points corresponding to the nontrivial Riemann zeros, providing strong evidence for the occurrence of DQPTs.

C. Measuring the Loschmidt amplitude

We consider a system, similar to the one described in Section II B, designed to measure the Loschmidt amplitude defined in Eq. (7). The composite system is initialized in the same state $\rho_0 = |\uparrow\rangle\langle\uparrow| \otimes \rho_s$, but now evolves under the coupling Hamiltonian $\mathcal{H}_{c2} = \frac{1}{2} \sigma_x \otimes (\mathcal{H}_0 - \dot{\theta}(t)\mathcal{I})$, which is one half of the Hamiltonian \mathcal{H}_c . The corresponding time-evolution operator is therefore $U(t) = \exp(-i \int_0^t \mathcal{H}_{c2} dt') = \exp(-\frac{i}{2} \int_0^t \mathcal{H}_c dt')$. Defining $A(t) = H_0 t - \theta(t)$, the density matrix after evolution is

$$\begin{aligned} U \rho_0 U^\dagger &= \frac{1}{2} \left[|+\rangle\langle+| \otimes \rho_s + e^{-iA(t)} |+\rangle\langle-| \otimes \rho_s \right. \\ &\quad \left. + e^{iA(t)} |-\rangle\langle+| \otimes \rho_s + |-\rangle\langle-| \otimes \rho_s \right], \quad (20) \end{aligned}$$

in which $|+\rangle = \frac{1}{\sqrt{2}}(|\uparrow\rangle + |\downarrow\rangle)$ and $|-\rangle = \frac{1}{\sqrt{2}}(|\uparrow\rangle - |\downarrow\rangle)$. The reduced density matrix of the probe qubit is

$$\rho_{\text{probe}} = \frac{1}{2} I + \frac{1}{2} \text{Re } S(t) \sigma_z + \frac{1}{2} \text{Im } S(t) \sigma_y, \quad (21)$$

in which

$$S(t) = \text{Tr}[e^{-iA(t)} \rho_s] = \frac{1}{\mathcal{Z}(\beta, H_0)} e^{i\theta(t)} \sum_{n=1}^N n^{-1/2-it}. \quad (22)$$

Consequently, measuring $\langle \sigma_z \rangle$ on the first qubit yields $\text{Re } S(t) = \mathcal{G}(\frac{1}{2}, t)$.

D. Construction of the quantum systems on gate-based quantum computers

In this subsection, we describe the construction of the target initial state $|\psi_0\rangle = \frac{1}{\mathcal{C}} \sum_{n=1}^N n^{-\beta/2} |n\rangle$ and the evolution operator $U(t) = e^{-i\mathcal{H}_0 t}$ with $\mathcal{H}_0 = \sum_{n=1}^N \log(n) |n\rangle\langle n|$ on a standard gate-based quantum computer. We begin with two preliminary lemmas. The first establishes a quantum oracle for evaluating polynomial functions, while the second provides a procedure for approximating logarithmic functions to required precision. Together, these results serve as building blocks for our main results: a method for constructing the initial state (Theorem 3) and an efficient implementation of the evolution operator (Theorem 4).

Lemma 1 (Polynomial oracle). *Let $O(f)$ denote an oracle implementing the transformation*

$$\sum_x \alpha_x |x\rangle |0\rangle \mapsto \sum_x \alpha_x |x\rangle |f(x)\rangle, \quad (23)$$

where $f(x)$ is a polynomial of degree at most D . Suppose the coefficients of f and the input x are specified to a_1 and a_2 significant digits, respectively. The output is encoded with r_1 integer qubits and r_2 fractional qubits. Then $O(f)$ can be implemented using $(D^2 a_2^2 + D^2 a_1 a_2 + D(r_1 + r_2))$ gates and $(2D a_2 + a_1)$ ancilla qubits.

Proof sketch. The oracle is implemented by sequentially constructing monomials x^d for $d \in [0, D]$, multiplying them by coefficients c_d , and summing the results (see Supplementary Note 3 for details).

Lemma 2 (Logarithm oracle). *Let L denote an oracle implementing the transformation*

$$\sum_{n=1}^N \alpha_n |n\rangle |0\rangle \mapsto \sum_{n=1}^N \alpha_n |n\rangle |\widetilde{\log n}\rangle, \quad (24)$$

where $\widetilde{\log n}$ approximates $\log n$ to within error η . Then L can be implemented using $\mathcal{O}((\log N)^3 \log^2(1/\eta))$ gates and $\mathcal{O}((\log N)^2 \log(1/\eta))$ ancilla qubits.

Proof sketch. The construction proceeds in two steps. First, a register of ancilla qubits identifies the interval

$$P_\nu : 3 \cdot 2^{\nu-1} \leq n < 3 \cdot 2^\nu, \quad 1 \leq \nu \leq \lceil \log(N/3) \rceil, \quad (25)$$

yielding a contribution $(\nu + 1)$ in $\log n$. Second, approximate the residual contribution

$$\log(1 + d), \quad d = n/2^{\nu+1} - 1, \quad (26)$$

to accuracy η using the polynomial oracle in Lemma 1. The result is encoded using $\log N$ qubits for the integer part and $\log(1/\eta)$ for the fractional part. Full details of the polynomial expansions and resource counts are provided in Supplementary Note 3.

1. Initial state preparation

The target initial state can be written (formally, up to normalization and coefficients) as

$$|\psi_0\rangle = |\psi_0\rangle_1 + |\psi_0\rangle_2 - |\psi_0\rangle_3. \quad (27)$$

We first construct of $|\psi_0\rangle_1$ using the Angle-preparation oracle U_m , and then recover the initial state via the linear combination of Unitary (LCU) method and post-selection. A complete proof is provided in Supplementary Note 4.

Theorem 1 (Truncated state preparation). *Let $\beta > 0$, $\beta \neq 1$, and let $n_0, n_1 \in \mathbb{N}$ with $n_1 - n_0 = 2^k$ for some integer $k > 0$. Define*

$$|\psi_0\rangle_1 = \frac{1}{C_1} \sum_{n=n_0}^{n_1-1} n^{-\beta/2} |n - n_0\rangle, \quad C_1 = \sqrt{\sum_{n=n_0}^{n_1-1} n^{-\beta}}. \quad (28)$$

Then $|\psi_0\rangle_1$ can be prepared on a standard gate-based quantum computer to precision $\varepsilon > 0$, using a number of gates and ancilla qubits bounded by

$$\text{Poly}(\log \varepsilon^{-1}, \log n_1, \log |1 - \beta|^{-1}, \beta, v), \quad (29)$$

where v denotes the number of significant digits used to represent β . The parameters are required to satisfy

$$c = \lceil \frac{1}{2} \log_{2\pi}(8\varepsilon^{-1}) \rceil, \quad n_0 > \lceil \beta + 2c \rceil. \quad (30)$$

Proof sketch. The construction adapts Grover's amplitude splitting method⁴³, replacing integrals with partial summations. The desired distribution is generated by k iterative amplitude splits. At step m ($0 \leq m \leq k - 1$), each bit string $w \in \{0, 1\}^m$ is divided into branches w_0 and w_1 , with a corresponding rotation angle $\theta_{w,m}$. All rotations for strings of the same length m can be applied in parallel; hence the main resource cost arises from constructing the angle-preparation oracle U_m .

Theorem 2 (Angle-preparation oracle U_m). *The unitary operator U_m implements*

$$\sum_{w \in \{0,1\}^m} \alpha_w |w\rangle |0\rangle \mapsto \sum_{w \in \{0,1\}^m} \alpha_w |w\rangle |\theta_{w,m}\rangle, \quad (31)$$

where the rotation angle $\theta_{w,m}$ is defined by

$$\theta_{w,m} = \arcsin \sqrt{S(a_1, b_1, \beta) / S(a_2, b_1, \beta)}, \quad (32)$$

in which $S(a, b, \sigma) = \sum_{n=a}^b n^{-\sigma}$ and

$$\begin{aligned} a_1 &= 2^{k-m-1}(2w+1) + n_0, \\ b_1 &= 2^{k-m-1}(2w+2) - 1 + n_0, \\ a_2 &= 2^{k-m}w + n_0. \end{aligned} \quad (33)$$

Then U_m can be implemented such that each rotation angle is estimated to within error ε/k , using

$$\text{Poly}(\log \varepsilon^{-1}, \log n_1, \log |1 - \beta|^{-1}, \beta, v) \quad (34)$$

gates and ancilla qubits, where v denotes the number of significant digits used to represent β .

Proof sketch. Each angle $\theta_{w,m}$ is obtained by a bit-wise bisection procedure. At iteration i , a trial angle $\theta_{g,i}$ is represented with i bits, and $\sin^2(\theta_{g,i})$ is compared to

the target ratio $S(a_1, b_1, \beta) / S(a_2, b_1, \beta)$. This comparison determines the i -th decimal digit of $\theta_{w,m}$. Repeating this procedure for $\mathcal{O}(\log(k/\varepsilon))$ iterations successively refines the approximation, yielding $\theta_{w,m}$ with precision ε/k . Furthermore, we show that both the computation of $\sin^2(\theta_{g,i})$ and the partial sums can be carried out with polynomial resources, which completes the proof.

Theorem 3 (Initial state preparation). *Let $\beta > 0$, $\beta \neq 1$ and $N \in \mathbb{N}$. Define*

$$|\psi_0\rangle = \frac{1}{C} \sum_{n=1}^N n^{-\beta/2} |n\rangle, \quad C = \sqrt{\sum_{n=1}^N n^{-\beta}}. \quad (35)$$

Then $|\psi_0\rangle$ can be prepared on a quantum computer to precision $\varepsilon > 0$, with success probability at least $(\frac{1}{2} - \frac{\varepsilon}{3})$. The required number of gates and ancilla qubits is bounded by

$$\text{Poly}(\log \varepsilon^{-1}, \log N, \log |1 - \beta|^{-1}, \beta, v), \quad (36)$$

where v denotes the number of significant digits used to represent β .

Proof sketch. The construction proceeds in three steps. First, prepare the auxiliary state using controlled rotations⁴⁴, noted that n_0 has only linear reliance on $\log(\varepsilon^{-1})$ and β :

$$|\psi_0\rangle_2 = \frac{1}{C_2} \sum_{n=1}^{n_0-1} n^{-\beta/2} |n\rangle. \quad (37)$$

Second, construct $|\psi_0\rangle_1$ using Theorem 1, and combine it with $|\psi_0\rangle_2$ via the LCU method, yielding

$$|\psi_0\rangle_1 + |\psi_0\rangle_2. \quad (38)$$

Third, post-select to eliminate the states with index $n > N$, given by:

$$|\psi_0\rangle_3 = \frac{1}{C_3} \sum_{n=N+1}^{n_1-1} n^{-\beta/2} |n\rangle, \quad (39)$$

yielding the desired state

$$|\psi_0\rangle = |\psi_0\rangle_1 + |\psi_0\rangle_2 - |\psi_0\rangle_3. \quad (40)$$

By appropriately choosing n_0 and n_1 , the procedure succeeds with probability at least $(\frac{1}{2} - \frac{\varepsilon}{3})$ and requires only polynomial resources.

2. Hamiltonian evolution

Theorem 4 (Evolution operator construction). *Define the time evolution operator*

$$U(t) = e^{-i\mathcal{H}_0 t}, \quad \mathcal{H}_0 = \sum_{n=1}^N \log n |n\rangle \langle n|, \quad (41)$$

where the evolution time t is specified with u significant digits. Then $U(t)$ can be implemented to precision ξ using

$$\text{Poly}(\log N, \log |t|, \log \xi^{-1}, u) \quad (42)$$

gates and ancilla qubits.

Proof sketch. The construction begins by using the logarithm oracle from Lemma 2, which maps

$$\sum_{n=1}^N \alpha_n |n\rangle |0\rangle \mapsto \sum_{n=1}^N \alpha_n |n\rangle |\widetilde{\log n}\rangle, \quad (43)$$

where $\widetilde{\log n}$ approximates $\log(n)$ to accuracy $O(\xi/|t|)$. The ancilla register storing $\log n$ requires $\log N$ qubits for the integer part and $\log(|t|/\xi)$ qubits for the fractional part. Controlled R_z rotations conditioned on these qubits then imprint the phase factor $e^{-it \log n}$ onto each computational basis state $|n\rangle$, thereby realizing $U(t)$ to precision ξ with polynomial overhead in the stated parameters (see Supplementary Note 5 for details).

The implementation of the controlled evolution

$$\exp(-i\mathcal{H}_{c2}t) = |\downarrow\rangle\langle\downarrow| \otimes U(t) \quad (44)$$

in the first system, as well as the time evolution

$$\begin{aligned} & \exp(-i \int \mathcal{H}_c dt) \\ & = H(e^{i\theta t} |\uparrow\rangle\langle\uparrow| \otimes U(t) + e^{-i\theta t} |\downarrow\rangle\langle\downarrow| \otimes U^\dagger(t)) H \end{aligned} \quad (45)$$

in the second system, exhibit the same complexity scaling. According to Theorem 4, both evolutions can be implemented to precision ξ using

$$\text{Poly}(\log N, \log |t|, \log \xi^{-1}, u) \quad (46)$$

gates and ancilla qubits.

E. The computational complexity of calculating the zeta Function in the critical strip

In classical computation, evaluating $\zeta(s)$ at large imaginary parts in the critical strip $0 < \beta < 1$ is notoriously challenging. The Riemann-Siegel formula can be expressed as:

$$\zeta(s) = \sum_{n=1}^x \frac{1}{n^s} + \chi(s) \sum_{n=1}^y \frac{1}{n^{1-s}} + O(x^{-\beta}) + O(|t|^{1/2-\beta} y^{\beta-1}),$$

with $2\pi xy = |t|$ and $\chi(s) = 2^s \pi^{s-1} \sin(\frac{\pi s}{2}) \Gamma(1-s)$. Setting $x = y = \sqrt{|t|/2\pi}$ yields

$$\zeta(s) = \sum_{n=1}^N n^{-s} + \chi(s) \sum_{n=1}^N n^{-(1-s)} + O(|t|^{-\beta/2}), \quad (47)$$

where $N = \lceil \sqrt{|t|/2\pi} \rceil$. Thus, the main computational challenge reduces to evaluating partial Dirichlet sums.

Using the quantum constructions in previous sections, we prepare the initial state

$$|\psi_0\rangle = \frac{1}{C} \sum_{n=1}^N n^{-\beta/2} |n\rangle, \quad C = \sqrt{\sum_{n=1}^N n^{-\beta}}, \quad (48)$$

and apply the evolution operator

$$U(t) = e^{-i\mathcal{H}_0 t}, \quad \mathcal{H}_0 = \sum_{n=1}^N \log n |n\rangle\langle n|. \quad (49)$$

The average accumulated phase factor can be obtained from the expectation values of $\sigma_x + i\sigma_y$ on an introduced probe qubit, yielding

$$\mathcal{L}(\beta, t) = \langle \psi_0 | e^{-i\mathcal{H}_0 t} | \psi_0 \rangle = \frac{1}{C^2} \sum_{n=1}^N n^{-s}. \quad (50)$$

For $0 < \beta < 1$, we have

$$C^2 = \sum_{n=1}^N n^{-\beta} \leq 1 + \int_1^N x^{-\beta} dx < \frac{N^{1-\beta}}{1-\beta}, \quad (51)$$

and $|\chi(s)| = \Theta(|t|^{1/2-\beta})$ (see Supplementary Note 7). Hence, to approximate $\zeta(\beta + it)$ with precision δ , it suffices to estimate the two partial sums $\sum_{n=1}^N n^{-s}$ and $\sum_{n=1}^N n^{-(1-s)}$ to precisions $\mathcal{O}(\delta)$ and $\mathcal{O}(\delta)|t|^{\beta-1/2}$ respectively. Therefore, the required precisions in the estimation of $\langle \sigma_x \rangle$ and $\langle \sigma_y \rangle$ of the probe qubits are $d_1 = (1-\beta)\mathcal{O}(\delta)/N^{1-\beta}$ and $d_2 = \beta\mathcal{O}(\delta)|t|^{\beta-\frac{1}{2}}/N^\beta$, respectively. To achieve an overall precision of d_1 and d_2 , the preparation of the initial state, the time evolution, and sampling the outputs must each be implemented to accuracies of order $\mathcal{O}(d_1)$ and $\mathcal{O}(d_2)$. By Theorem 3 and Theorem 4, substituting ε and ξ with $\mathcal{O}(d_1)$ and $\mathcal{O}(d_2)$ yield gate and ancilla resource requirements for initial state preparation and evolution bounded by

$$\text{Poly}(\log \delta^{-1}, \log |t|, \log(1-\beta)^{-1}, \log \beta^{-1}, v), \quad (52)$$

and

$$\text{Poly}(\log \delta^{-1}, \log |t|, \log(1-\beta)^{-1}, \log \beta^{-1}, u), \quad (53)$$

respectively, where u, v denote the number of significant digits of t and β .

Let $\zeta'(s)$ denote the derivative of $\zeta(s)$, which can be bounded by $\text{Poly}(|t|, |1-\beta|^{-1}, \beta^{-1})$ (see Supplementary Note 6 for details). Thus, setting u, v as $\text{Poly}(\log \delta^{-1}, \log |t|, \log(1-\beta)^{-1}, \log \beta^{-1})$ ensures that rounding errors contribute at most $\mathcal{O}(\delta)$. Substituting these bounds into the previous bounds gives gate and ancilla qubit costs \mathcal{R}_{c1} and \mathcal{R}_{c2} for both summations:

$$\text{Poly}(\log \delta^{-1}, \log |t|, \log(1-\beta)^{-1}, \log \beta^{-1}). \quad (54)$$

If $\langle \sigma_x \rangle$ and $\langle \sigma_y \rangle$ are estimated by direct sampling, sample complexity scales as $\mathcal{O}(d_1^{-2})$ and $\mathcal{O}(d_2^{-2})$. With amplitude amplification or quantum amplitude estimation, this can be reduced to $\mathcal{O}(d_1^{-1})$ and $\mathcal{O}(d_2^{-1})$. Since $N = \Theta(\sqrt{|t|})$, the required number of samples is bounded by

$$\begin{aligned} \mathcal{R}_{s1} &= \mathcal{O}(\delta^{-1})(1-\beta)^{-1}|t|^{(1-\beta)/2}, \\ \mathcal{R}_{s2} &= \mathcal{O}(\delta^{-1})\beta^{-1}|t|^{(1-\beta)/2}. \end{aligned} \quad (55)$$

Hence, the overall complexity $\mathcal{R}_o = \mathcal{R}_{c1}\mathcal{R}_{s1} + \mathcal{R}_{c2}\mathcal{R}_{s2}$ is bounded by:

$$\delta^{-1}|t|^{(1-\beta)/2} \text{Poly}(\log \delta^{-1}, \log |t|, (1-\beta)^{-1}, \beta^{-1}). \quad (56)$$

Next, we consider the task of locating and verifying nontrivial zeros. These zeros are symmetric with respect to the critical line $\beta = \frac{1}{2}$, and there is a known zero-free region, known as Korobov-Vinogradov zero-free region, which takes the form³⁸:

$$\beta > 1 - \frac{1}{\mathcal{O}((\log |t|)^{2/3} (\log \log |t|)^{1/3})}. \quad (57)$$

Thus, we focus on the region satisfying

$$\frac{1}{2} \leq \beta \leq 1 - \frac{1}{\mathcal{O}((\log |t|)^{2/3} (\log \log |t|)^{1/3})}, \quad (58)$$

for which the complexity bound simplifies to

$$\delta^{-1}|t|^{(1-\beta)/2}\text{Poly}(\log \delta^{-1}, \log |t|). \quad (59)$$

Data and code availability

Data and code are available from the corresponding author upon reasonable request.

Acknowledgements

S.W. acknowledges Beijing Nova Program (Grants No. 20230484345). This work is supported by the National Natural Science Foundation of China (62571050, 12275117), Guangdong Basic and Applied Basic Research Foundation (2022B1515020074), and Shenzhen Science and Technology Program (RCYX20200714114522109 and KQTD20200820113010023). We thank Feihao Zhang for the helpful discussion.

Author contributions

T.X., G.L.L. and S.W. supervised the project. S.W. proposed the initial theoretical idea and developed the theoretical framework together with Q.L. and T.X.. Y.Z. performed the experiments under the supervision of T.X. W.Y., P.G., F.N. contributed to the theoretical analysis, while C.W. and J.S. contributed to the experimental work. All authors participated in the preparation of the manuscript.

Competing interests

The authors declare no competing interests.

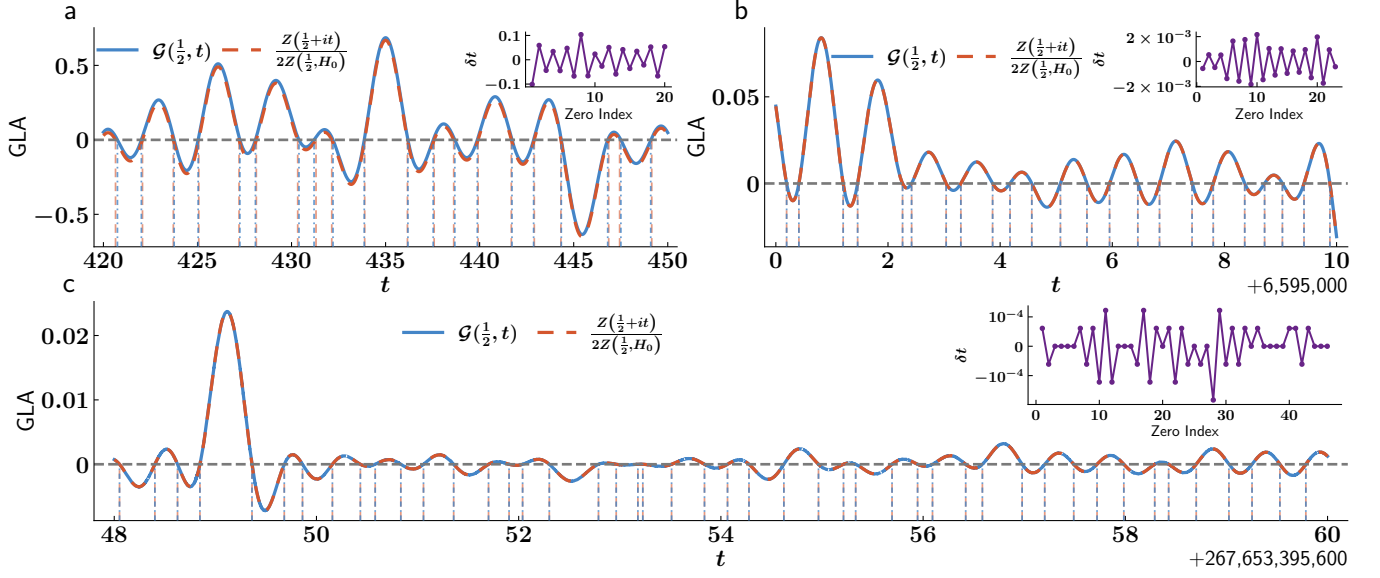


FIG. 5. **Generalized Loschmidt amplitude $\mathcal{G}(\frac{1}{2}, t)$ across different imaginary part regions.** **a** Nontrivial zeros with imaginary parts in the range $[420, 450]$, corresponding to the 216-th to 235-th zeros, obtained using a 3-spin quantum system. **b** Nontrivial zeros with imaginary parts in the range $[6.595 \times 10^6, 6.595 \times 10^6 + 10]$, corresponding to the 13,502,344-th to 13,502,366-th zeros, obtained using a 10-spin quantum system. **c** Nontrivial zeros with imaginary parts in the range $[267,653,395,648, 267,653,395,660]$, corresponding to the $(10^{12} - 3)$ -th to $(10^{12} + 43)$ -th zeros, obtained using a 18-spin quantum system. The blue solid line shows the simulated $\mathcal{G}(\frac{1}{2}, t)$, while the red dashed line show $Z(\frac{1}{2} + it) / (2Z(\frac{1}{2}, H_0))$. Vertical red dashed lines mark the exact Riemann zeros, and blue dashed and dotted lines mark the zeros estimated by the quantum system. Insets show the deviation δt between the exact zeros and estimated zeros, which decreases with increasing t .

Region of β	Sample complexity \mathcal{R}_s	Total complexity $\mathcal{R}_c \mathcal{R}_s$
$0 < \beta < 1$	$\mathcal{O}(\delta^{-1}) t ^{(1-\beta)/2}(\beta^{-1} + (1-\beta)^{-1})$	$\delta^{-1} t ^{(1-\beta)/2}\text{Poly}(\log \delta^{-1}, \log t , (1-\beta)^{-1}, \beta^{-1})$
Possible zero region	$\mathcal{O}(\delta^{-1}) t ^{(1-\beta)/2}(\beta^{-1} + (1-\beta)^{-1})$	$\delta^{-1} t ^{(1-\beta)/2}\text{Poly}(\log \delta^{-1}, \log t)$
$\beta = \frac{1}{2}$	$\mathcal{O}(\delta^{-1}) t ^{1/4}$	$\delta^{-1} t ^{1/4}\text{Poly}(\log \delta^{-1}, \log(t))$
Classical method	$\sim t $ (Alternating series) ⁴⁵ , $\sim t ^{1/2}$ (Riemann-Siegel formula) ³²	

TABLE II. **Complexity bounds of the quantum algorithm for evaluating $\zeta(\beta + it)$ with precision δ across different regions, compared with classical approaches.** The “possible zero region”, defined in Eq. (58), is the regime of interest for locating and verifying nontrivial zeros.

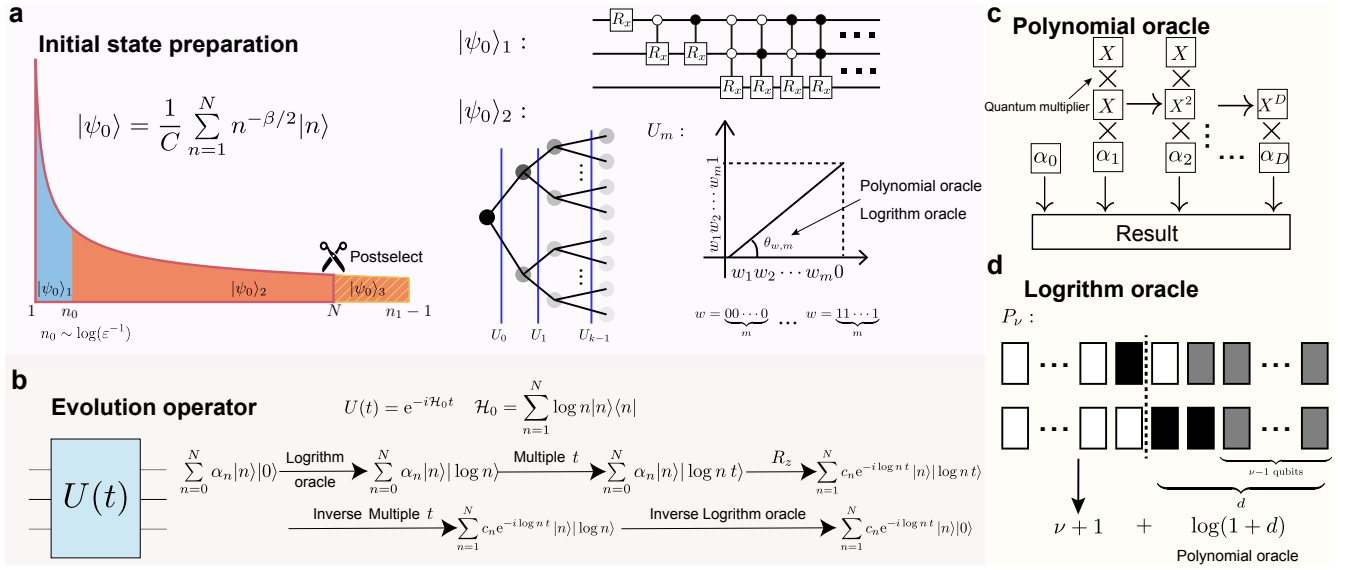


FIG. 6. **Construction of the quantum system on a gate-based quantum computer.** **a**, The initial state is prepared as $|\psi_0\rangle = |\psi_0\rangle_1 + |\psi_0\rangle_2 - |\psi_0\rangle_3$ (normalization omitted). The components $|\psi_0\rangle_1$, $|\psi_0\rangle_2$, and $|\psi_0\rangle_3$ correspond to the blue, orange, and slashed yellow regions, respectively. The states $|\psi_0\rangle_1$ and $|\psi_0\rangle_2$ are generated using controlled rotations and Grover's amplitude-splitting method, respectively. **b**, The time-evolution operator is realized in five sequential steps. **c**, **d**, The polynomial and logarithmic oracles serve as preliminary blocks for implementing the time-evolution operator and preparing the initial state.

Supplementary information for "The Riemann Hypothesis Emerges in Dynamical Quantum Phase Transitions"

Notation

For clarity, throughout this Supplementary Information, we use ‘log’ to denote the base-2 logarithm, and ‘ln’ to denote the natural logarithm (base e). All variables s are assumed to satisfy $\text{Re}(s) > 0$ and $\text{Re}(s) \neq 1$, ensuring the applicability of the alternating Dirichlet series. β denote the real part of s and t denote the imaginary part of s .

The Big-O notation $\mathcal{O}(\cdot)$ represents the worst-case upper bound, while the Big-Theta notation $\Theta(\cdot)$ denotes the exact asymptotic behavior. The notation $\text{Poly}(\cdot)$ signifies that the growth follows a polynomial function of the input.

The symbol $\|\cdot\|$ denotes the Euclidean norm on state vectors. The distance between two pure quantum states $|\psi_a\rangle$ and $|\psi_b\rangle$ is defined as $d(|\psi_a\rangle, |\psi_b\rangle) = \min_{\theta \in \mathbb{R}} \|\psi_a - e^{i\theta} \psi_b\| = \sqrt{2(1 - |\langle \psi_a | \psi_b \rangle|)}$, which satisfies the triangle inequality. The distance between two unitary operators is defined as $D(U_1, U_2) = \max_{|\psi\rangle} d(U_1|\psi\rangle, U_2|\psi\rangle)$, which is the worst-case distance over all input states $|\psi\rangle$. We say that a quantum state (or unitary operator) is prepared to precision κ if its distance from the corresponding ideal target state (or ideal unitary) is at most κ .

Supplementary Note 1: Asymptotic behavior of $S_N(s)$

The N -term partial sum of the alternating Dirichlet series is

$$S_N(s) = \sum_{n=1}^N \frac{(-1)^{n-1}}{n^s}. \quad (1.1)$$

Case 1. At the nontrivial zeros of the zeta function, we have $S_N(s) = -R_N(s)$, where

$$R_N(s) = \sum_{n=N+1}^{\infty} \frac{(-1)^{n-1}}{n^s}. \quad (1.2)$$

Each term has the following integral representation,

$$\frac{1}{n^s} = \frac{1}{\Gamma(s)} \int_0^{\infty} \tau^{s-1} e^{-n\tau} d\tau, \quad (1.3)$$

yielding

$$R_N(s) = \sum_{n=N+1}^{\infty} \frac{(-1)^{n-1}}{n^s} = \frac{1}{\Gamma(s)} \int_0^{\infty} \tau^{s-1} \sum_{n=N+1}^{\infty} (-1)^{n-1} e^{-n\tau} d\tau = \frac{(-1)^N}{\Gamma(s)} \int_0^{\infty} \frac{\tau^{s-1} e^{-(N+1)\tau}}{1 + e^{-\tau}} d\tau. \quad (1.4)$$

Using the identity

$$\frac{1}{1 + e^{-\tau}} = \frac{1}{2} + \frac{1}{2} \tanh\left(\frac{\tau}{2}\right), \quad (1.5)$$

we obtain

$$R_N(s) = \frac{(-1)^N}{\Gamma(s)} \left[\frac{1}{2} \int_0^{\infty} \tau^{s-1} e^{-(N+1)\tau} d\tau + \frac{1}{2} \int_0^{\infty} \tau^{s-1} e^{-(N+1)\tau} \tanh\left(\frac{\tau}{2}\right) d\tau \right]. \quad (1.6)$$

Let us define

$$M := \frac{1}{2} \int_0^{\infty} \tau^{s-1} e^{-(N+1)\tau} d\tau = \frac{1}{2} \Gamma(s) (N+1)^{-s}, \quad J := \frac{1}{2} \int_0^{\infty} \tau^{s-1} e^{-(N+1)\tau} \tanh\left(\frac{\tau}{2}\right) d\tau. \quad (1.7)$$

This leads to

$$R_N(s) = \frac{(-1)^N}{\Gamma(s)} (M + J) = (-1)^N \left(\frac{1}{2(N+1)^s} + \frac{J}{\Gamma(s)} \right), \quad (1.8)$$

We now show that for sufficiently large N ,

$$|J| \leq \frac{1}{4} \Gamma(s) (N+1)^{-\beta}, \quad s = \beta + it. \quad (1.9)$$

Fix $A > 0$, which depends on s but not on N , and split the integral for J at $\tau = A/(N+1)$:

$$J = \frac{1}{2} \left(\int_0^{A/(N+1)} \tau^{s-1} e^{-(N+1)\tau} \tanh\left(\frac{\tau}{2}\right) d\tau + \int_{A/(N+1)}^{\infty} \tau^{s-1} e^{-(N+1)\tau} \tanh\left(\frac{\tau}{2}\right) d\tau \right) := \frac{1}{2} (I_1 + I_2). \quad (1.10)$$

For I_1 , we apply the inequality $|\tanh(\tau/2)| \leq |\tau/2|$, so

$$|I_1| \leq \int_0^{A/(N+1)} \tau^{\beta-1} e^{-(N+1)\tau} \frac{\tau}{2} d\tau = \frac{1}{2} (N+1)^{-(\beta+1)} \int_0^A u^\beta e^{-u} du = C_1(\beta, A) (N+1)^{-(\beta+1)}. \quad (1.11)$$

Here, $C_1(\beta, A) := \frac{1}{2} \int_0^A u^\beta e^{-u} du$ is a constant depending on A and β . For I_2 , we use the trivial bound $|\tanh(\tau/2)| \leq 1$, so

$$|I_2| \leq \int_{A/(N+1)}^\infty \tau^{\beta-1} e^{-(N+1)\tau} d\tau = (N+1)^{-\beta} \int_A^\infty u^{\beta-1} e^{-u} du = C_2(\beta, A) (N+1)^{-\beta}. \quad (1.12)$$

Here $C_2(\beta, A) := \int_A^\infty u^{\beta-1} e^{-u} du$ is also a constant that depends on A and β .

Since $\Gamma(s)$ is non-vanishing and $C_2(\beta, A) \rightarrow 0$ as $A \rightarrow \infty$, we can choose A large enough so that

$$C_2(\beta, A) \leq \frac{1}{4} |\Gamma(s)|. \quad (1.13)$$

Thus,

$$|I_2| \leq \frac{1}{4} |\Gamma(s)| (N+1)^{-\beta}. \quad (1.14)$$

Combining the two contributions gives

$$|J| \leq \frac{1}{2} (|I_1| + |I_2|) \leq \frac{1}{2} \left(C_1(\beta, A) (N+1)^{-(\beta+1)} + \frac{1}{4} |\Gamma(s)| (N+1)^{-\beta} \right). \quad (1.15)$$

Consequently, for all $N \geq N_0 := \lceil 4C_1(\beta, A)/|\Gamma(s)| \rceil$,

$$|J| \leq \frac{1}{4} |\Gamma(s)| (N+1)^{-\beta}, \quad \left| \frac{J}{\Gamma(s)} \right| \leq \frac{1}{4} (N+1)^{-\beta}. \quad (1.16)$$

Substituting this bound into Equation (1.8) gives for $N \geq N_0$,

$$\frac{1}{4} (N+1)^{-\beta} \leq |R_N(s)| \leq \frac{3}{4} (N+1)^{-\beta}. \quad (1.17)$$

Therefore,

$$\lim_{N \rightarrow \infty} -\frac{1}{\log N} \ln |S_N(s)| = \lim_{N \rightarrow \infty} -\frac{1}{\log N} \ln |R_N(s)| = \beta \ln 2. \quad (1.18)$$

Case 2. For s with $\zeta(s) \neq 0$, the partial sums converge, and in particular

$$\lim_{N \rightarrow \infty} S_N(s) = (1 - 2^{1-s}) \zeta(s) \neq 0. \quad (1.19)$$

It follows that

$$-\lim_{N \rightarrow \infty} \frac{1}{\log N} \ln |S_N(s)| = 0. \quad (1.20)$$

Thus, we obtain the final result:

$$-\lim_{N \rightarrow \infty} \frac{1}{\log N} \ln |S_N(s)| = \begin{cases} \beta \ln 2, & \text{if } \zeta(s) = 0, \\ 0, & \text{if } \zeta(s) \neq 0. \end{cases} \quad (1.21)$$

Supplementary Note 2: Asymptotic behavior of $\mathcal{Z}(\beta, \mathcal{H}_0)$

The partition function can be written as

$$\mathcal{Z}(\beta, \mathcal{H}_0) = \sum_{n=1}^N n^{-\beta}. \quad (2.1)$$

Case 1. For $\beta > 1$, $\mathcal{Z}(\beta, \mathcal{H}_0)$ converges as

$$\lim_{N \rightarrow \infty} \mathcal{Z}(\beta, \mathcal{H}_0) = \zeta(\beta). \quad (2.2)$$

Thus,

$$\lim_{N \rightarrow \infty} -\frac{1}{\log N} \ln \mathcal{Z}(\beta, \mathcal{H}_0) = 0. \quad (2.3)$$

Case 2. For $0 < \beta < 1$, the series diverges. Specifically,

$$\int_1^{N+1} x^{-\beta} dx \leq \sum_{n=1}^N n^{-\beta} \leq 1 + \int_1^N x^{-\beta} dx, \quad (2.4)$$

which simplifies to

$$\frac{(N+1)^{1-\beta} - 1}{1-\beta} \leq \mathcal{Z}(\beta, \mathcal{H}_0) \leq 1 + \frac{N^{1-\beta} - 1}{1-\beta}, \quad (2.5)$$

yielding

$$-\lim_{N \rightarrow \infty} \frac{1}{\log N} \ln \mathcal{Z}(\beta, \mathcal{H}_0) = (\beta - 1) \ln 2. \quad (2.6)$$

Thus,

$$-\lim_{N \rightarrow \infty} \frac{1}{\log N} \ln \mathcal{Z}(\beta, \mathcal{H}_0) = \begin{cases} (\beta - 1) \ln 2, & 0 < \beta < 1, \\ 0, & \beta > 1. \end{cases} \quad (2.7)$$

Supplementary Note 3: Construction of the preliminary oracles

This section details the construction of polynomial and logarithm oracles, which serve as foundational components for subsequent quantum state preparation and time evolution operators in our quantum algorithms.

Lemma 3.1 (Polynomial oracle (Methods, Lemma 1)). *Let $O(f)$ denote an oracle implementing the transformation*

$$\sum_x \alpha_x |x\rangle |0\rangle \mapsto \sum_x \alpha_x |x\rangle |f(x)\rangle, \quad (3.1)$$

where $f(x)$ is a polynomial of degree at most D . Suppose the coefficients of f and the input x are specified to a_1 and a_2 significant digits, respectively. The output is encoded with r_1 integer qubits and r_2 fractional qubits. Then $O(f)$ can be implemented using

$$\mathcal{O}(D^2 a_2^2 + D^2 a_1 a_2 + D(r_1 + r_2)) \text{ gates, and } (2Da_2 + a_1) \text{ ancilla qubits.}$$

Proof. Write the polynomial as $f(n) = \sum_{d=0}^D c_d n^d$. Evaluation proceeds through sequential construction of the monomials x^d , multiplication by coefficients c_d , and accumulation of the results.

Step 1: Computation of Monomials. Multiplying an m_1 -qubit register by an m_2 -qubit register requires $\mathcal{O}(m_1 m_2)$ gates and $\mathcal{O}(m_1 + m_2)$ qubits using quantum schoolbook multiplication⁴⁶. To compute x^{d+1} from x^d , a da_2 -qubit register (storing x^d) is multiplied by an a_2 -qubit register (storing x). The total gate cost for generating monomials up to degree D is

$$2 \sum_{d=1}^{D-1} a_2 \cdot da_2 = \mathcal{O}(D^2 a_2^2), \quad (3.2)$$

where the factor 2 arises from uncomputing intermediate results and resetting ancilla qubits.

Step 2: Multiplication by coefficients. Multiplying a degree- d monomial (which requires da_2 qubits) by c_d costs $\mathcal{O}(da_1 a_2)$ gates. Summing over all degrees gives

$$2 \sum_{d=1}^D da_1 a_2 = \mathcal{O}(D^2 a_1 a_2), \quad (3.3)$$

again with the factor 2 from uncomputation.

Step 3: Accumulation of output. The results are accumulated into an output register of size $r_1 + r_2$. Each of the $D+1$ additions costs $\mathcal{O}(r_1 + r_2)$ gates, yielding a total gate cost of $\mathcal{O}(D(r_1 + r_2))$. Adding all contributions yields a total gate complexity

$$\mathcal{O}(D^2 a_2^2 + D^2 a_1 a_2 + D(r_1 + r_2)). \quad (3.4)$$

During computation, at most Da_2 qubits are used for monomial storage and $(Da_2 + a_1)$ for intermediate products, giving a total ancilla requirement of $(2Da_2 + a_1)$. \square

Lemma 3.2 (Logarithm oracle (Methods, Lemma 2)). *Let L denote an oracle implementing the transformation*

$$\sum_{n=1}^N \alpha_n |n\rangle |0\rangle \mapsto \sum_{n=1}^N \alpha_n |n\rangle |\widetilde{\log(n)}\rangle, \quad (3.5)$$

where $\widetilde{\log(n)}$ approximates $\log(n)$ to within error η . Then L can be implemented using $\mathcal{O}((\log N)^3 \log^2(1/\eta))$ gates and $\mathcal{O}((\log N)^2 \log(1/\eta))$ ancilla qubits.

Proof. We proceed constructively.

Step 1: Input Partitioning. Define $k_1 = \lceil \log(\frac{N+1}{3}) \rceil$. For $3 \leq n < 3 \cdot 2^{k_1}$, partition the integers into k_1 subsets, defined as

$$P_\nu : \quad 3 \cdot 2^{\nu-1} \leq n_\nu < 3 \cdot 2^\nu, \quad 1 \leq \nu \leq k_1. \quad (3.6)$$

Each $3 \leq n \leq N$ lies in exactly one partition P_ν . For $n_\nu \in P_\nu$, define

$$d = \frac{n_\nu - 2^{\nu+1}}{2^{\nu+1}}, \quad -\frac{1}{4} \leq d < \frac{1}{2}. \quad (3.7)$$

This allows the logarithm to be expressed as

$$\log(n_\nu) = \log(2^{\nu+1}) + \log(1+d). \quad (3.8)$$

Step 2: Taylor expansion of $\log(1+d)$. Using the Taylor series expansion for $\log(1+d)$, we have:

$$\log(1+d) = \frac{1}{\ln 2} \sum_{j=1}^{\infty} \frac{(-1)^{j+1}}{j} d^j. \quad (3.9)$$

The remainder after l_1 terms satisfies

$$\left| \sum_{j=l_1+1}^{\infty} \frac{(-1)^{j+1}}{j} d^j \right| \leq \sum_{j=l_1+1}^{\infty} \frac{1}{j} \left(\frac{1}{2}\right)^j \leq \frac{1}{2^{l_1}}. \quad (3.10)$$

Hence, truncating after $l_1 = \lceil \log(1/\eta) \rceil + 2$ terms yields an approximation error of less than $\frac{\eta}{2}$. Coefficients stored to $\lceil \log(2/\eta) \rceil$ fractional bits introduce an additional rounding error bounded by

$$\frac{\eta}{2} \left(1 + \frac{1}{2} + \left(\frac{1}{2}\right)^2 + \dots\right) \leq \frac{\eta}{2}, \quad (3.11)$$

giving total error of less than η . The resulting approximation

$$\widetilde{\log(n_\nu)} = \nu + 1 + \frac{1}{\ln(2)} \sum_{j=1}^{l_1} \frac{(-1)^{j+1}}{j} d^j \quad (3.12)$$

is thus approximated within error η .

The partition index ν is determined using multi-controlled operations that compare n with partition bounds. Each such comparison uses at most $\mathcal{O}(k_1)$ Toffoli gates and $\mathcal{O}(k_1)$ ancilla qubits. A flag register composing of at most $\mathcal{O}(k_1)$ qubits marks the unique partition P_ν containing n . This flag controls addition of the corresponding polynomial output to the output register. Exactly one flag is set for each input across $3 \leq n \leq N$.

For each ν , Equation (3.12) is a degree- l_1 polynomial in d , with coefficients specified to $\lceil \log(2/\eta) \rceil$ qubits and input d to $(k_1 + 2)$ significant digits. The output requires $(\lceil \log k_1 \rceil + 2)$ integer qubits and $\lceil \log(1/\eta) \rceil$ fractional qubits. Applying Lemma 3.1, evaluating this polynomial within a partition requires

$$\mathcal{O}(l_1^2 k_1^2 + l_1^2 k_1 \log(2/\eta) + l_1(\log(k_1) + \log(1/\eta))) = \mathcal{O}(k_1^2 \log^2(1/\eta)) \quad (3.13)$$

gates, and

$$2l_1 k_1 + \log(1/\eta) = \mathcal{O}(k_1 \log(1/\eta)) \quad (3.14)$$

ancilla qubits. Summing over all k_1 partitions gives total resource requirements:

$$\mathcal{O}(k_1^3 \log^2(1/\eta)) = \mathcal{O}((\log N)^3 \log^2(1/\eta)) \text{ gates}, \quad \mathcal{O}(k_1^2 \log(1/\eta)) = \mathcal{O}((\log N)^2 \log(1/\eta)) \text{ ancilla qubits}. \quad (3.15)$$

The special cases $n = 1, 2$ can be handled separately at negligible cost. \square

Supplementary Note 4: Construction of the initial state

This section details the construction of the initial state, which is outlined as follows:

Our first key result is provided in Theorem 4.2 (Methods, Theorem 1), which describes the preparation of the truncated state $|\psi_0\rangle_1$. Central to this construction is the angle-preparation oracle (Methods, Theorem 2) that computes the required rotation angles. Its action is defined in Definition 4.3 and its implementation is outlined in Theorem 4.4. A central subroutine of this oracle is the evaluation of a zeta function related partial sum (Lemma 4.7), built upon Proposition 4.5 with detailed calculations given in Propositions 4.8 and 4.9.

Our second key result, Theorem 4.11 (Methods, Theorem 3), presents the construction of our initial state $|\psi_0\rangle$. Starting with the truncated state $|\psi_0\rangle_1$ prepared in Theorem 4.2, we extend it via the Linear Combination of Unitaries (LCU) method to combine it with $|\psi_0\rangle_2$ (Corollary 4.10); a final post-selection removes the high-index component $|\psi_0\rangle_3$, yielding the desired initial state.

Definition 4.1. The controlled-rotation gate \mathcal{CR} implements the transformation

$$\sum_{\theta} \alpha_{\theta} |\theta\rangle |0\rangle \mapsto \sum_{\theta} \alpha_{\theta} |\theta\rangle (\cos \theta |0\rangle + \sin \theta |1\rangle). \quad (4.1)$$

It can be implemented using a sequence of controlled- R_x rotations, each conditioned on a qubit of the register encoding θ , followed by a phase gate on the target qubit.

Theorem 4.2 (Truncated state preparation (Methods, Theorem 1)). Let $\beta > 0$, $\beta \neq 1$, and let $n_0, n_1 \in \mathbb{N}$ with $n_1 - n_0 = 2^k$ for some integer $k > 0$. Define

$$|\psi_0\rangle_1 = \frac{1}{C_1} \sum_{n=n_0}^{n_1-1} n^{-\beta/2} |n - n_0\rangle, \quad C_1 = \sqrt{\sum_{n=n_0}^{n_1-1} n^{-\beta}}. \quad (4.2)$$

Then $|\psi_0\rangle_1$ can be prepared on a standard gate-based quantum computer to precision $\varepsilon > 0$, using a number of gates and ancilla qubits bounded by

$$\text{Poly}\left(\log(1/\varepsilon), \log(n_1), \log\left(\frac{1}{|1-\beta|}\right), \beta, v\right), \quad (4.3)$$

where v denotes the number of significant digits used to represent β . The parameters are required to satisfy

$$c = \left\lceil \frac{1}{2} \log_{2\pi} \left(\frac{8}{\varepsilon} \right) \right\rceil, \quad n_0 > \lceil \beta + 2c \rceil. \quad (4.4)$$

Proof sketch. We adapt Grover's recursive amplitude-splitting method⁴³, replacing integration with partial summation. The 2^k computational basis states are encoded on k qubits initialized in $|0\rangle^{\otimes k}$. At iteration step m ($0 \leq m \leq k-1$), each bit string $w \in \{0, 1\}^m$ is split into two branches $w0$ and $w1$. Define

$$c_w = \frac{1}{C} \sqrt{\sum_{i=0}^{2^{k-m}-1} (2^{k-m}w + i + n_0)^{-\beta}}. \quad (4.5)$$

Normalization is preserved, as

$$c_{w0} = \frac{1}{C} \sqrt{\sum_{i=0}^{2^{k-m-1}-1} (2^{k-m}w + i + n_0)^{-\beta}}, \quad c_{w1} = \frac{1}{C} \sqrt{\sum_{i=0}^{2^{k-m-1}-1} (2^{k-m}(w+1) + i + n_0)^{-\beta}}, \quad (4.6)$$

satisfy $c_{w0}^2 + c_{w1}^2 = c_w^2$. For each w , we compute a rotation angle $\theta_{w,m}$ such that the amplitude split $c_w \mapsto (c_{w0}, c_{w1})$ can be implemented by a \mathcal{CR} gate acting on the next qubit. All rotations corresponding to strings of the same length m are applied in parallel. The transformation at step m is written as

$$\begin{aligned} & \sum_{w \in \{0,1\}^m} c_w |w\rangle |0\rangle^{\otimes(k-m)} |0\rangle \\ & \xrightarrow{U_m} \sum_w c_w |w\rangle |0\rangle^{\otimes(k-m)} |\theta_{w,m}\rangle \\ & \xrightarrow{\mathcal{CR}} \sum_w c_w |w\rangle (\cos \theta_{w,m} |0\rangle + \sin \theta_{w,m} |1\rangle) |0\rangle^{\otimes(k-m-1)} |\theta_{w,m}\rangle \\ & \xrightarrow{U_m^\dagger} \sum_w (c_{w0} |w0\rangle + c_{w1} |w1\rangle) |0\rangle^{\otimes(k-m-1)} |0\rangle. \end{aligned} \quad (4.7)$$

Here, U_m denote an oracle that computes $\theta_{w,m}$ into an angle register, which is uncomputed after applying \mathcal{CR} gate. Iterating the transformation in Equation (4.7) for $m = 0, 1, \dots, k-1$ yields the desired state

$$|\psi_0\rangle = \frac{1}{C} \sum_{n=n_0}^{n_1-1} n^{-\beta/2} |n - n_0\rangle. \quad (4.8)$$

Thus, the central task reduces to constructing U_m , defined as follows. □

Definition 4.3 (Angle-preparation oracle U_m). The gate U_m implements the transformation

$$\sum_{w \in \{0,1\}^m} \alpha_w |w\rangle |0\rangle \mapsto \sum_{w \in \{0,1\}^m} \alpha_w |w\rangle |\theta_{w,m}\rangle, \quad (4.9)$$

where the rotation angle $\theta_{w,m}$ satisfies

$$\tan^2(\theta_{w,m}) = \frac{c_{w1}^2}{c_{w0}^2} = \frac{\sum_{i=0}^{2^{k-m-1}-1} (2^{k-m-1}(2w+1) + i + n_0)^{-\beta}}{\sum_{i=0}^{2^{k-m-1}-1} (2^{k-m-1}(2w) + i + n_0)^{-\beta}} = \frac{S(2^{k-m-1}(2w+1) + n_0, 2^{k-m-1}(2w+2) - 1 + n_0, \beta)}{S(2^{k-m-1}(2w) + n_0, 2^{k-m-1}(2w+1) - 1 + n_0, \beta)}, \quad (4.10)$$

with

$$S(a, b, \beta) = \sum_{n=a}^b n^{-\beta}. \quad (4.11)$$

Equivalently,

$$\begin{aligned} \theta_{w,m} &= \arctan\left(\sqrt{\frac{S(2^{k-m-1}(2w+1) + n_0, 2^{k-m-1}(2w+2) - 1 + n_0, \beta)}{S(2^{k-m-1}(2w) + n_0, 2^{k-m-1}(2w+1) - 1 + n_0, \beta)}}}\right) \\ &= \arcsin\left(\sqrt{\frac{S(2^{k-m-1}(2w+1) + n_0, 2^{k-m-1}(2w+2) - 1 + n_0, \beta)}{S(2^{k-m-1}(2w) + n_0, 2^{k-m-1}(2w+2) - 1 + n_0, \beta)}}}\right). \end{aligned} \quad (4.12)$$

Notation. In practice, U_m computes an approximation $\tilde{\theta}_{w,m}$, which results in an error in the state preparation. The deviation between the ideal and approximate states at step m is bounded as follows:

$$\begin{aligned} &\left\| \sum_w c_w |w\rangle (\cos(\theta_{w,m})|0\rangle + \sin(\theta_{w,m})|1\rangle) |0\rangle^{\otimes(k-m-1)} |0\rangle - \sum_w c_w |w\rangle (\cos(\tilde{\theta}_{w,m})|0\rangle + \sin(\tilde{\theta}_{w,m})|1\rangle) |0\rangle^{\otimes(k-m-1)} |0\rangle \right\| \\ &= \left\| \sum_w c_w |w\rangle [(\cos(\tilde{\theta}_{w,m}) - \cos(\theta_{w,m}))|0\rangle + (\sin(\tilde{\theta}_{w,m}) - \sin(\theta_{w,m}))|1\rangle] \right\| \\ &= \sqrt{\sum_w c_w^2 \cdot 4 \sin^2\left(\frac{\tilde{\theta}_{w,m} - \theta_{w,m}}{2}\right)} \\ &\leq \max_w |\tilde{\theta}_{w,m} - \theta_{w,m}|. \end{aligned} \quad (4.13)$$

To achieve overall precision ε , each $\theta_{w,m}$ must be computed with an error of at most ε/k over all m . The \mathcal{CR} gate is decomposed into controlled- R_x rotations conditioned on the qubits encoding $\theta_{w,m}$, followed by a phase gate, requiring $\mathcal{O}(\log(k/\varepsilon))$ gates and no ancilla qubits. Therefore, the dominant resource cost comes from implementing U_m to an accuracy of ε/k .

Theorem 4.4 (Implementation of oracle U_m (Methods, Theorem 2)). *The gate U_m , as defined in Definition 4.3, can be implemented such that each rotation angle is estimated to within error ε/k , using a number of gates and ancilla qubits bounded by*

$$\text{Poly}\left(\log(1/\varepsilon), \log(n_1), \log \frac{1}{|1-\beta|}, \beta, v\right), \quad (4.14)$$

where v denotes the number of significant digits used to represent β .

Proof. The angle $\theta_{w,m}$, represented with $\log(k/\varepsilon)$ qubits, is determined using a bisection procedure applied iteratively on each qubit. For a trial angle θ_g , we compare

$$\sin^2(\theta_g) S(2^{k-m-1}2w + n_0, 2^{k-m-1}(2w+2) - 1 + n_0, \beta), \quad (4.15)$$

$$\text{with } S(2^{k-m-1}(2w+1) + n_0, 2^{k-m-1}(2w+2) - 1 + n_0, \beta). \quad (4.16)$$

This comparison decides whether $\theta_{w,m} > \theta_g$. After $\log(k/\varepsilon)$ comparison, $\theta_{w,m}$ is computed to within error ε/k . Define

$$d = \sin^2(\theta_g) S(2^{k-m-1} \cdot 2w + n_0, 2^{k-m-1}(2w+2) - 1 + n_0, \beta) - S(2^{k-m-1}(2w+1) + n_0, 2^{k-m-1}(2w+2) - 1 + n_0, \beta). \quad (4.17)$$

Since $S(a, b, \beta) \geq n_1^{-\beta}$ and relevant angles θ satisfy $\theta + \frac{\varepsilon}{k} < \frac{\pi}{4}$, consider two angles differing by at least ε/k . The difference in $\sin^2 \theta$:

$$\sin^2\left(\theta + \frac{\varepsilon}{k}\right) - \sin^2(\theta) = (\sin\left(\theta + \frac{\varepsilon}{k}\right) - \sin(\theta))(\sin\left(\theta + \frac{\varepsilon}{k}\right) + \sin(\theta)) > \frac{\sqrt{2}\varepsilon}{2k} \sin\left(\frac{\varepsilon}{k}\right) > \frac{\varepsilon^2}{2k^2}. \quad (4.18)$$

Thus, angles differing by ε/k yield a difference in d of at least $\frac{\varepsilon^2}{2k^2} n_1^{-\beta}$. To distinguish such angles correctly, the error in d must be less than $\frac{\varepsilon^2}{2k^2} n_1^{-\beta}$. Since $S(a, b, \beta) \leq n_1$, requirements:

- (1) computing S to precision $\frac{\varepsilon^2 n_1^{-\beta}}{12k^2}$,
- (2) $\sin^2 \theta_g$ to precision $\frac{\varepsilon^2 n_1^{-1-\beta}}{12k^2}$,

ensures the total error meets this requirement.

Step 1: Calculation of $\sin^2(\theta)$. Using the expansion

$$\sin^2(\theta) = \frac{1 - \cos(2\theta)}{2} = \sum_{n=1}^{\infty} d_n \theta^{2n}, \quad d_n = \frac{(-1)^{n+1} 2^{2n}}{2(2n)!}, \quad (4.19)$$

we approximate $\sin^2(\theta)$ for $\theta < \frac{\pi}{4}$. Truncating after $l_2 > 5$ terms, the error is:

$$\frac{(\frac{\pi}{2})^{2l_2+2}}{2(2l_2+2)!} < \frac{(\frac{\pi}{2})^{2l_2+2}}{(\frac{2l_2+2}{e})^{2l_2+2}} = \left(\frac{e\pi}{4l_2+4}\right)^{2l_2+2} < \left(\frac{1}{2}\right)^{l_2}, \quad (4.20)$$

using Stirling's approximation. To achieve precision $\frac{\varepsilon^2 n_1^{-1-\beta}}{24k^2}$, we choose:

$$l_2 = 2 \log\left(\frac{k}{\varepsilon}\right) + (1 + \beta) \log(n_1) + 5. \quad (4.21)$$

Storing coefficients d_n to precision $\frac{\varepsilon^2 n_1^{-1-\beta}}{96k^2}$ ensures that the rounding error is bounded by:

$$\frac{\varepsilon^2 n_1^{-1-\beta}}{96k^2} \left(\frac{\pi}{4} + \left(\frac{\pi}{4}\right)^2 + \dots\right) < \frac{\varepsilon^2 n_1^{-1-\beta}}{24k^2}. \quad (4.22)$$

Thus, the total truncation and rounding error is within $\frac{\varepsilon^2 n_1^{-1-\beta}}{12k^2}$, satisfying the requirement **(1)**.

The expression approximating $\sin^2(\theta)$ is a polynomial of degree $2l_2$. The parameter θ is encoded using $\log\left(\frac{k}{\varepsilon}\right)$ qubits, the coefficients require $\log\left(\frac{\varepsilon^2 n_1^{-1-\beta}}{96k^2}\right)$ qubits, and the output requires $\frac{\varepsilon^2 n_1^{-1-\beta}}{12k^2}$ qubits. By Lemma 3.1, the gate complexity is

$$4 \log^2\left(\frac{k}{\varepsilon}\right) l_2^2 + 4 \log\left(\frac{k}{\varepsilon}\right) \log\left(\frac{96k^2 n_1^{1+\beta}}{\varepsilon^2}\right) l_2^2 + 2l_2 \log\left(\frac{12k^2 n_1^{1+\beta}}{\varepsilon^2}\right) = \text{Poly}(\log(n_1), \log(1/\varepsilon), \beta), \quad (4.23)$$

and the ancilla qubit count is

$$4l_2 \log\left(\frac{k}{\varepsilon}\right) + \log\left(\frac{96k^2 n_1^{1+\beta}}{\varepsilon^2}\right) = \text{Poly}(\log(n_1), \log(1/\varepsilon), \beta). \quad (4.24)$$

Step 2: Estimation of S . We will prove Lemma 4.7, which states that the partial sum $S(a, b, \beta)$ can be computed to precision ϵ with:

$$\text{Poly}\left(\log(1/\epsilon), \log n_1, \log\left(\frac{1}{|1-\beta|}\right), v\right) \quad (4.25)$$

gates and ancilla qubits, where v denotes the significant digits of β . To satisfy requirement **(2)**, we set $\epsilon = \frac{\varepsilon^2 n_1^{-\beta}}{12k^2}$ and the complexity becomes:

$$\text{Poly}\left(\log\left(\frac{12k^2 n_1^\beta}{\varepsilon^2}\right), \log(n_1), \log\left(\frac{1}{|1-\beta|}\right), v\right) = \text{Poly}\left(\log(1/\varepsilon), \log(n_1), \log\left(\frac{1}{|1-\beta|}\right), \beta, v\right).$$

Conclusively, we give a total count of required resources for constructing U_m . The bisection procedure requires $\lceil \log(k/\varepsilon) \rceil$ comparisons to compute $\theta_{w,m}$ to precision ε/k . Each comparison involves two evaluations of S (for the partial sums in (4.15) and (4.16)) and one evaluation of $\sin^2 \theta_g$. Thus, the total resource cost for U_m is multiplied by a factor of $\mathcal{O}(\log(k/\varepsilon))$, which is absorbed into the overall polynomial complexity. Combining the resource costs from Steps 1 and 2 (concluded in Equation (4.23),(4.24),(4.25)), the total gate and ancilla qubit complexity for implementing the oracle U_m is bounded by

$$\text{Poly}\left(\log(1/\varepsilon), \log(n_1), \log\frac{1}{|1-\beta|}, \beta, v\right), \quad (4.26)$$

as stated. As a preliminary step of Lemma 4.7, an approximation of S is introduced in Proposition 4.5. \square

Proposition 4.5 (Euler–Maclaurin approximation of S). *For $\beta > 0$, $\beta \neq 1$, and integers $a \leq b$, there exists an approximation $\widetilde{S}(a, b, \beta)$ to the partial sum $S(a, b, \beta) = \sum_{n=a}^b n^{-\beta}$, such that*

$$\left|S(a, b, \beta) - \widetilde{S}(a, b, \beta)\right| < \frac{\epsilon}{2}, \quad (4.27)$$

where

$$\widetilde{S}(a, b, \beta) = \frac{1}{1-\beta} (b^{1-\beta} - a^{1-\beta}) + \frac{a^{-\beta} + b^{-\beta}}{2} - \sum_{r=1}^{l_3} \frac{B_{2r} \Gamma(\beta + 2r - 1)}{(2r)! \Gamma(\beta)} (b^{-\beta-2r+1} - a^{-\beta-2r+1}), \quad (4.28)$$

with $l_3 = \lceil \frac{1}{2} \log_{2\pi} \frac{8}{\epsilon} \rceil$, provided $a > \lceil \beta + 2m \rceil$.

Proof. Recall the Euler–Maclaurin summation formula:

$$\sum_{k=a}^b f(k) = \int_a^b f(x) dx + \frac{f(a) + f(b)}{2} + \sum_{r=1}^{l_3} \frac{B_{2r}}{(2r)!} \left(f^{(2r-1)}(b) - f^{(2r-1)}(a) \right) + R_{l_3}, \quad (4.29)$$

where B_{2r} are Bernoulli Numbers, and the remainder is given by

$$R_{l_3} = \frac{(-1)^{l_3+1}}{(2l_3)!} \int_a^b B_{2l_3}(x - [x]) f^{(2l_3)}(x) dx. \quad (4.30)$$

Setting $f(x) = x^{-\beta}$, we have

$$\begin{aligned} S(a, b, \beta) &= \int_a^b x^{-\beta} dx + \frac{a^{-\beta} + b^{-\beta}}{2} + \sum_{r=1}^{l_3} \frac{B_{2r}}{(2r)!} (-1)^{2r-1} \left(\prod_{i=0}^{2r-2} (\beta + i) \right) (b^{-\beta-2r+1} - a^{-\beta-2r+1}) + R_{l_3} \\ &= \frac{1}{1-\beta} (b^{1-\beta} - a^{1-\beta}) + \frac{a^{-\beta} + b^{-\beta}}{2} - \sum_{r=1}^{l_3} \frac{B_{2r} \Gamma(\beta + 2r - 1)}{(2r)! \Gamma(\beta)} (b^{-\beta-2r+1} - a^{-\beta-2r+1}) + R_{l_3}, \end{aligned} \quad (4.31)$$

in which the reminder term is given by

$$R_{l_3} = \frac{(-1)^{l_3+1}}{(2l_3)!} \int_a^b B_{2l_3}(x - [x]) \frac{\Gamma(\beta + 2l_3)}{\Gamma(\beta)} x^{-\beta-2l_3} dx. \quad (4.32)$$

Using the bound on Bernoulli numbers:

$$\frac{2(2l_3)!}{(2\pi)^{2l_3}} \frac{1}{1 - 2^{-2l_3}} < |B_{2l_3}| = \frac{2(2l_3)!}{(2\pi)^{2l_3}} \zeta(2l_3) < \frac{2(2l_3)!}{(2\pi)^{2l_3}} \frac{1}{1 - 2^{1-2l_3}}, \quad (4.33)$$

we obtain

$$\begin{aligned} |R_{l_3}| &\leq \frac{|B_{2l_3}|}{(2l_3)!} \beta(\beta+1) \cdots (\beta+2l_3-1) \int_a^b x^{-\beta-2l_3} dx \\ &= \left| \frac{\beta(\beta+1) \cdots (\beta+2l_3-1) B_{2l_3} (a^{-\beta-2l_3+1} - b^{-\beta-2l_3+1})}{(2l_3)! (\beta+2l_3-1)} \right| \\ &< \frac{\beta(\beta+1) \cdots (\beta+2l_3-2) 2a^{-\beta-2l_3+1}}{(2\pi)^{2l_3} (1 - 2^{1-2l_3})} \\ &< \frac{4}{(2\pi)^{2l_3}} \frac{\beta(\beta+1) \cdots (\beta+2l_3-2)}{a^{\beta+2l_3-1}}. \end{aligned} \quad (4.34)$$

Thus, choosing $l_3 = \lceil \frac{1}{2} \log_{2\pi} \frac{8}{\epsilon} \rceil$ guarantees $|R_{l_3}| < \frac{\epsilon}{2}$, provided $a > [\beta + 2l_3]$. \square

Corollary 4.6. *The Bernoulli numbers satisfy $B_0 = 1$, and for all $q \geq 1$,*

$$\sum_{p=0}^q \binom{q+1}{p} B_p = 0. \quad (4.35)$$

The Bernoulli numbers can be computed efficiently using the Akiyama–Tanigawa algorithm⁴⁷, with a complexity $O(p^2)$ for computing B_p .

Lemma 4.7 ($\widehat{S(a, b, \beta)}$ calculation oracle). *Let $S(\beta)$ be an oracle implementing*

$$\sum_{n_0 \leq a \leq b \leq n_1 - 1} \alpha_{ab} |a\rangle |b\rangle |0\rangle \mapsto \sum_{n_0 \leq a \leq b \leq n_1 - 1} \alpha_{ab} |a\rangle |b\rangle |\widehat{S(a, b, \beta)}\rangle, \quad (4.36)$$

where $\widehat{S(a, b, \beta)}$ is an $\frac{\epsilon}{2}$ -approximation of $S(a, b, \beta)$ as defined in Equation (4.28), and therefore an ϵ -approximation of $S(a, b, \beta)$. Then $S(\beta)$ can be constructed using

$$\text{Poly}(\log(1/\epsilon), \log(n_1), \log\left(\frac{1}{1-\beta}\right), v) \quad (4.37)$$

gates and ancilla qubits, where $l_3 = \lceil \frac{1}{2} \log_{2\pi} \frac{8}{\epsilon} \rceil$, $n_0 > \beta + 2l_3$, and v is the number of significant digits of β .

Proof sketch. We compute $\widehat{S(a, b, \beta)}$, as defined in Equation (4.28), with an error of at most $\epsilon/2$ by evaluating its

exponential terms and finite Bernoulli-series sums:

$$\begin{aligned}
\widetilde{S}(a, b, \beta) &= b^{-\beta-2l_3+1} \left(\frac{1}{1-\beta} b^{2l_3} + \frac{1}{2} b^{2l_3-1} - \sum_{r=1}^{l_3} \frac{B_{2r} \Gamma(\beta+2r-1)}{(2r)! \Gamma(\beta)} b^{2l_3-2r} \right) \\
&\quad - a^{-\beta-2l_3+1} \left(\frac{1}{1-\beta} a^{2l_3} - \frac{1}{2} a^{2l_3-1} - \sum_{r=1}^{l_3} \frac{B_{2r} \Gamma(\beta+2r-1)}{(2r)! \Gamma(\beta)} a^{2l_3-2r} \right) \\
&= b^{-\beta-2l_3+1} P_b(\beta) - a^{-\beta-2l_3+1} P_a(\beta),
\end{aligned} \tag{4.38}$$

where

$$\begin{aligned}
P_b(\beta) &= \frac{1}{1-\beta} b^{2l_3} + \frac{1}{2} b^{2l_3-1} - \sum_{r=1}^{l_3} \frac{B_{2r} \Gamma(\beta+2r-1)}{(2r)! \Gamma(\beta)} b^{2l_3-2r}, \\
P_a(\beta) &= \frac{1}{1-\beta} a^{2l_3} - \frac{1}{2} a^{2l_3-1} - \sum_{r=1}^{l_3} \frac{B_{2r} \Gamma(\beta+2r-1)}{(2r)! \Gamma(\beta)} a^{2l_3-2r}.
\end{aligned}$$

Define the r -th term in the sum of $P_b(\beta)$:

$$T_b(r) = \frac{B_{2r} \Gamma(\beta+2r-1)}{(2r)! \Gamma(\beta)} b^{2l_3-2r}.$$

Then the ratio of consecutive terms is

$$\left| \frac{T_b(r+1)}{T_b(r)} \right| = \left| \frac{B_{2r+2}}{B_{2r}} \right| \frac{(\beta+2r-1)(\beta+2r)}{(2r+2)(2r+1)} \frac{1}{b^2}.$$

Using the bounds of Bernoulli number

$$\frac{2(2r)!}{(2\pi)^{2r}} \frac{1}{1-2^{-2r}} < |B_{2r}| = \frac{2(2r)!}{(2\pi)^{2r}} \zeta(2r) < \frac{2(2r)!}{(2\pi)^{2r}} \frac{1}{1-2^{1-2r}}, \tag{4.39}$$

for $b > \beta + 2l_3$, we obtain:

$$\left| \frac{T_b(r+1)}{T_b(r)} \right| < \frac{(\beta+2r-1)(\beta+2r)(1-2^{-2r})}{(2\pi)^2 b^2 (1-2^{1-2(r+1)})} < \frac{1}{2\pi^2}.$$

Thus the Bernoulli series decreases geometrically,

$$\left| \sum_{r=1}^{l_3} \frac{B_{2r} \Gamma(\beta+2r-1)}{(2r)! \Gamma(\beta)} b^{2l_3-2r} \right| < \left| \frac{B_2 \beta b^{2l_3-2}}{2 \left(1 - \frac{1}{2\pi^2}\right)} \right| < \frac{\beta b^{2l_3-2}}{6} < \frac{b^{2l_3-1}}{2}. \tag{4.40}$$

By combining the fact that $\frac{b^{2l_3-1}}{2} < \frac{b^{2l_3}}{2|1-\beta|}$, we obtain

$$|P_b(\beta)| < \frac{2b^{2l_3}}{|1-\beta|}, \tag{4.41}$$

and similarly,

$$|P_a(\beta)| < \frac{2a^{2l_3}}{|1-\beta|}. \tag{4.42}$$

Hence, to achieve overall precision $\frac{\epsilon}{2}$, it suffices to:

1. Compute $a^{-\beta-2l_3+1}$ and $b^{-\beta-2l_3+1}$ to precisions:

$$\frac{\epsilon|1-\beta|}{16a^{2l_3}} \quad \text{and} \quad \frac{\epsilon|1-\beta|}{16b^{2l_3}}, \tag{4.43}$$

respectively. We will prove in Proposition 4.8 that these require at most

$$\text{Poly}(\log(n_1), \log\left(\frac{1}{|1-\beta|}\right), \log(1/\epsilon), v) \tag{4.44}$$

gates and ancilla qubits.

2. Compute the polynomial-Bernoulli sums $P_a(\beta)$ and $P_b(\beta)$ to precision $\frac{\epsilon}{8}$, since $a^{-\beta-2l_3+1}$ and $b^{-\beta-2l_3+1}$ are both smaller than 1. We will prove in Proposition 4.9 that these require:

$$\text{Poly}(\log(1/\epsilon), \log(n_1), \log\left(\frac{1}{|1-\beta|}\right), v) \tag{4.45}$$

gates and ancilla qubits.

3. Perform final multiplications and additions to combine terms. As the exponential terms and Bernoulli-series sums require at most

$$\log\left(\frac{16n_1^{2l_3}}{|1-\beta|\epsilon}\right), \quad \log\left(\frac{2n_1^{2l_3}}{|1-\beta|}\right) + \log\left(\frac{8}{\epsilon}\right)$$

significant qubits, respectively.

Conclusively, the total number of required gates and ancilla qubits can be bounded by

$$\text{Poly}(\log(1/\epsilon), \log(n_1), \log\left(\frac{1}{|1-\beta|}\right), v), \quad (4.46)$$

given that $l_3 = \lceil \frac{1}{2} \log_{2\pi} \frac{8}{\epsilon} \rceil$. Hence the Lemma follows. Next, we detail Proposition 4.8 and Proposition 4.9. \square

Proposition 4.8. *The oracles*

$$\sum_{b=n_0}^{n_1-1} \alpha_b |b\rangle |0\rangle \mapsto \sum_{b=n_0}^{n_1-1} \alpha_b |b\rangle |\widetilde{b^{-\beta-2l_3+1}}\rangle \quad \text{and} \quad \sum_{a=n_0}^{n_1-1} \alpha_a |a\rangle |0\rangle \mapsto \sum_{a=n_0}^{n_1-1} \alpha_a |a\rangle |\widetilde{a^{-\beta-2l_3+1}}\rangle \quad (4.47)$$

can be constructed with error bounds

$$|\widetilde{b^{-\beta-2l_3+1}} - b^{-\beta-2l_3+1}| < \frac{\epsilon|1-\beta|}{16b^{2l_3}}, \quad |\widetilde{a^{-\beta-2l_3+1}} - a^{-\beta-2l_3+1}| < \frac{\epsilon|1-\beta|}{16a^{2l_3}}, \quad (4.48)$$

using

$$\text{Poly}(\log(n_1), \log\left(\frac{1}{|1-\beta|}\right), \log(1/\epsilon), v) \quad (4.49)$$

gates and ancilla qubits, where $n_0 > \beta + 2l_3$, and v denotes the number of significant digits of β .

Proof. We focus on constructing the oracle for $\widetilde{b^{-\beta-2l_3+1}}$; the case for a is analogous. Writing $b^{-\beta-2l_3+1} = 2^{-(\beta+2l_3-1)\log b}$, the computation proceeds by approximating $\log b$, multiplying by $-(\beta+2l_3-1)$, and exponentiating. We require the approximation errors from the logarithm and from the exponentiation to be both bounded by $\frac{\epsilon|1-\beta|}{32b^{2l_3}}$, so that the total error is bounded by $\frac{\epsilon|1-\beta|}{16b^{2l_3}}$.

Step 1: Approximating $\log(b)$. If $(\beta+2l_3-1)|\log(\widetilde{b}) - \log(b)| < \frac{1}{2}$, then

$$\begin{aligned} & |2^{-(\beta+2l_3-1)\log(b)} - 2^{-(\beta+2l_3-1)\log(\widetilde{b})}| \\ &= 2^{-(\beta+2l_3-1)\log(b)} \left| 1 - 2^{-(\beta+2l_3-1)(\log(\widetilde{b}) - \log(b))} \right| \\ &< b^{-\beta-2l_3+1} (\beta+2l_3-1) |\log(\widetilde{b}) - \log(b)|, \end{aligned} \quad (4.50)$$

since $|1-2^x| \leq |x|$ for $|x| \leq \frac{1}{2}$. To bound this error by $\frac{\epsilon|1-\beta|}{32b^{2l_3}}$, it suffices to compute $\log(b)$ to precision

$$\frac{\epsilon|1-\beta|}{32b^{2l_3}} \frac{b^{\beta+2l_3-1}}{(\beta+2l_3-1)} = \frac{b^{\beta-1}\epsilon|1-\beta|}{32(\beta+2l_3-1)} > \frac{1}{32} n_1^{-2} |1-\beta| \epsilon, \quad (4.51)$$

which satisfies $\frac{1}{32} n_1^{-2} |1-\beta| \epsilon (\beta+2l_3-1) < \frac{1}{32} \epsilon < \frac{1}{2}$. Therefore, we set the required qubit of precision as

$$p_1 = \log\left(32n_1^2 \frac{1}{|1-\beta|} \frac{1}{\epsilon}\right) = 5 + 2\log(n_1) + \log\left(\frac{1}{|1-\beta|}\right) + \log\left(\frac{1}{\epsilon}\right). \quad (4.52)$$

By Lemma 3.2, computing $\log(b)$ to p_1 digits of precision requires

$$\mathcal{O}(\log(n_1)^3 p_1^2) \text{ gates and } \mathcal{O}(\log(n_1)^2 p_1) \text{ ancilla qubits.}$$

Step 2: Multiplication with $\beta + 2l_3 - 1$. Multiplying $\log b$ by $\beta + 2l_3 - 1$, which are represented to at most $\log(n_1) + p_1$ and $\log(n_0) + v$ bits respectively, requires:

$$(\log(n_1) + p_1)(\log(n_0) + v) \text{ gates and } (\log(n_1) + p_1) + (\log(n_0) + v) \text{ ancilla qubits,}$$

where v is the number of significant digits of β .

Step 3: Exponentiation. Decompose

$$b^{-\beta-2l_3+1} = 2^{\lfloor -(\beta+2l_3-1)\log(b) \rfloor} \cdot 2^{\{-\beta-2l_3+1\}\log(b)}, \quad (4.53)$$

where $\lfloor y \rfloor$ denote the nearest integer of y and $\{y\} = y - \lfloor y \rfloor$ denote the fractional part. The fractional exponential is evaluated by:

$$2^x = e^{\ln 2 \cdot x} = \sum_{n=0}^{\infty} \frac{(\ln 2)^n}{n!} x^n, \quad -\frac{1}{2} \leq x < \frac{1}{2}. \quad (4.54)$$

To bound the total error by $\frac{\epsilon|1-\beta|}{32b^{2l_3}}$, we target an error of

$$\frac{\epsilon|1-\beta|}{32b^{2l_3}} \frac{1}{\sqrt{2}b^{-(\beta+2l_3-1)}} = \frac{b^{\beta+2l_3-1}\epsilon|1-\beta|}{32\sqrt{2}b^{2l_3}} > \frac{1}{64}b^{\beta-1}|1-\beta|\epsilon > \frac{1}{64}n_1^{-1}|1-\beta|\epsilon. \quad (4.55)$$

in fractional exponential. Let

$$l_4 = \log\left(64n_1 \frac{1}{|1-\beta|} \frac{1}{\epsilon}\right) = 6 + \log(n_1) + \log\left(\frac{1}{|1-\beta|}\right) + \log\left(\frac{1}{\epsilon}\right). \quad (4.56)$$

Because $|x| \leq \frac{1}{2}$, truncating the exponential series at degree l_4 gives an error

$$\frac{2(\ln 2/2)^{l_4}}{(l_4)!} < \frac{1}{2^{l_4+1}} = \frac{1}{128}n_1^{-1}|1-\beta|\epsilon. \quad (4.57)$$

With coefficients stored with $l_4 + 1$ fractional qubits, the rounding error is at most

$$\frac{1}{128}n_1^{-1}|1-\beta|\epsilon\left(1 + \frac{1}{2} + \frac{1}{4} + \dots\right) \leq \frac{1}{128}n_1^{-1}|1-\beta|\epsilon \leq \frac{1}{128}n_1^{\beta-1}|1-\beta|\epsilon, \quad (4.58)$$

yielding a total error at most $\frac{1}{64}n_1^{-1}|1-\beta|\epsilon$.

By Lemma 3.1, evaluating the degree- l_4 polynomial in the argument $\{-(\beta + 2l_3 - 1)\log(b)\}$, which is represented with at most $(p_1 + \log(n_1) + \log(n_0) + v)$ bits through multiplication, and with coefficients stored with $l_4 + 1$ qubits, to achieve precision $\frac{\epsilon|1-\beta|}{32b^{2l_3}}$ requires

$$\begin{aligned} & l_4^2(p_1 + \log(n_0) + \log(n_1) + v)^2 + l_4^2(p_1 + \log(n_0) + \log(n_1) + v)(l_4 + 1) + \log\left(\frac{32b^{2l_3}}{|1-\beta|\epsilon}\right)l_4 \\ & = \text{Poly}\left(\log(n_1), \log\left(\frac{1}{|1-\beta|}\right), \log\left(\frac{1}{\epsilon}\right), v\right) \end{aligned} \quad (4.59)$$

gates, and

$$2(p_1 + \log(n_0) + \log(n_1) + v)^2l_4 + l_4 + 1 = \text{Poly}\left(\log(n_1), \log\left(\frac{1}{|1-\beta|}\right), \log\left(\frac{1}{\epsilon}\right), v\right) \quad (4.60)$$

ancilla qubits. Thus, combine the three parts and the claimed resource bounds follow. \square

Proposition 4.9. *The oracles*

$$\sum_{b=n_0}^{n_1-1} \alpha_b |b\rangle|0\rangle \mapsto \sum_{b=n_0}^{n_1-1} \alpha_b |b\rangle|P_b(\beta)\rangle \quad \text{and} \quad \sum_{a=n_0}^{n_1-1} \alpha_a |a\rangle|0\rangle \mapsto \sum_{a=n_0}^{n_1-1} \alpha_a |a\rangle|P_a(\beta)\rangle, \quad (4.61)$$

where

$$\begin{aligned} P_b(\beta) &= \frac{1}{1-\beta}b^{2l_3} + \frac{1}{2}b^{2l_3-1} - \sum_{r=1}^{l_3} \frac{B_{2r}\Gamma(\beta+2r-1)}{(2r)!\Gamma(\beta)}b^{2l_3-2r}, \\ P_a(\beta) &= \frac{1}{1-\beta}a^{2l_3} - \frac{1}{2}a^{2l_3-1} - \sum_{r=1}^{l_3} \frac{B_{2r}\Gamma(\beta+2r-1)}{(2r)!\Gamma(\beta)}a^{2l_3-2r}, \end{aligned} \quad (4.62)$$

can be constructed to precision $\frac{\epsilon}{8}$ using

$$\text{Poly}\left(\log(1/\epsilon), \log(n_1), \log\left(\frac{1}{|1-\beta|}\right)\right) \quad (4.63)$$

gates and ancilla qubits, in which $n_0 > \beta + 2l_3$.

Proof. We focus on constructing the oracle for $P_b(\beta)$, as the case for $P_a(\beta)$ is analogous. All the coefficients are stored with precision $\frac{\epsilon}{16n_1^{2l_3}}$, so the total rounding is bounded by

$$\frac{\epsilon}{16n_1^{2l_3}}(b^{2l_3} + b^{2l_3-1} + \dots) < \frac{\epsilon}{16n_1^{2l_3}}2b^{2l_3} \leq \frac{\epsilon}{8}. \quad (4.64)$$

Hence the required number of qubit for each coefficient is at most

$$p_2 = \log\left(\frac{16n_1^{2l_3}}{\epsilon}\right) = \log(1/\epsilon) + 4 + 2l_3 \log(n_1). \quad (4.65)$$

The polynomial in Equation (4.62) has degree $2l_3$, with input b requiring at most $\log(n_1)$ qubits, and the output targeted to precision $\frac{\epsilon}{8}$ with absolute magnitude bounded by $\log\left(\frac{2}{|1-\beta|}n_1^{2l_3}\right)$. Lemma 3.1 implies that this computation

can be performed using at most

$$\begin{aligned} & l_3^2 \log^2(n_1) + l_3^2 \log(n_1)p_2 + l_3 \left(\log\left(\frac{2}{|1-\beta|} n_1^{2l_3}\right) + \log\left(\frac{8}{\epsilon}\right) \right) \\ & = \text{Poly}\left(\log(n_1), \log\left(\frac{1}{|1-\beta|}\right), \log\left(\frac{1}{\epsilon}\right)\right) \end{aligned} \quad (4.66)$$

gates, and

$$2l_3 \log(n_1) + p_2 = \text{Poly}(\log(n_1), \log(1/\epsilon)) \quad (4.67)$$

ancilla qubits. \square

Corollary 4.10 (Extended state preparation). *Let $\beta > 0$, $\beta \neq 1$. Define*

$$|\psi_0\rangle_e = \frac{1}{C} \sum_{n=1}^{n_1-1} n^{-\beta/2} |n\rangle, \quad C = \sqrt{\sum_{n=1}^{n_1-1} n^{-\beta}}, \quad (4.68)$$

where $c = \lceil \frac{1}{2} \log_{2\pi} \frac{24}{\epsilon} \rceil$, $n_0 - 1$ is the smallest power of 2 greater than $\lceil \beta + 2c \rceil$, and $n_1 - n_0$ is a power of 2. Then the state $|\psi_0\rangle_e$ can be prepared on a gate-based quantum computer to precision $\epsilon > 0$ using

$$\text{Poly}(\log(1/\epsilon), \log(n_1), \log\left(\frac{1}{|1-\beta|}\right), \beta, v), \quad (4.69)$$

gates and ancilla qubits, where v is the number of significant digits used to represent β .

Proof. By Theorem 4.2, the truncated state

$$|\psi_0\rangle = \frac{1}{C} \sum_{n=n_0}^{n_1-1} n^{-\beta/2} |n\rangle \quad (4.70)$$

can be prepared to precision $\frac{\epsilon}{3}$ with

$$\text{Poly}(\log(1/\epsilon), \log(n_1), \log\left(\frac{1}{|1-\beta|}\right), \beta, v) \quad (4.71)$$

gates and ancilla qubits, for $c = \lceil \frac{1}{2} \log_{2\pi} \frac{24}{\epsilon} \rceil$ and n_0 greater than $\lceil \beta + 2c \rceil + 1$. Following the approach of direct amplitude splitting⁴⁴, we can also prepare

$$|\psi_1\rangle = \frac{1}{C_1} \sum_{n=1}^{n_0-1} n^{-\beta/2} |n\rangle, \quad (4.72)$$

to precision $\frac{\epsilon}{3}$, using $\text{Poly}(n_0, \log(1/\epsilon))$ gates. An auxiliary qubit coherently combines the two states:

$$\frac{|0\rangle + \gamma|1\rangle}{\sqrt{\gamma^2 + 1}} |0\rangle \rightarrow \frac{|0\rangle|\psi_0\rangle + \gamma|1\rangle|\psi_1\rangle}{\sqrt{\gamma^2 + 1}}. \quad (4.73)$$

Applying a Hadamard gate gives:

$$\xrightarrow{H} \frac{(|0\rangle + |1\rangle)|\psi_0\rangle + \gamma(|0\rangle - |1\rangle)|\psi_1\rangle}{\sqrt{2\gamma^2 + 2}} = \frac{|0\rangle(|\psi_0\rangle + \gamma|\psi_1\rangle) + |1\rangle(|\psi_0\rangle - \gamma|\psi_1\rangle)}{\sqrt{2\gamma^2 + 2}}. \quad (4.74)$$

Here, $\gamma = \frac{C_1}{C} = \sqrt{\frac{S(1, n_0-1, \beta)}{S(n_0, n_1-1, \beta)}}$, where the denominator is estimated via Euler-Maclaurin summation method and the numerator is computed directly. If the ancilla is measured in $|0\rangle$, the desired normalized superposition is obtained. If not, a correction step—using an additional register for comparison with n_0 and a controlled- Z operation—restores the target state. The comparator writes a 1 in an auxiliary qubit iff the index is smaller than n_0 . The process is listed as follows:

$$(|\psi_0\rangle - \gamma|\psi_1\rangle)|0\rangle \xrightarrow{\text{comparator}} |\psi_0\rangle|0\rangle - \gamma|\psi_1\rangle|1\rangle \xrightarrow{\text{controlled-}Z} |\psi_0\rangle|0\rangle + \gamma|\psi_1\rangle|1\rangle \xrightarrow{\text{undo comparator}} (|\psi_0\rangle + \gamma|\psi_1\rangle)|0\rangle. \quad (4.75)$$

If γ is approximated by $\tilde{\gamma}$, the error is bounded by

$$\begin{aligned} & \left\| \frac{|\psi_0\rangle + \tilde{\gamma}|\psi_1\rangle}{\sqrt{1 + \tilde{\gamma}^2}} - \frac{|\psi_0\rangle + \gamma|\psi_1\rangle}{\sqrt{1 + \gamma^2}} \right\| = \sqrt{2 - 2 \frac{1 + \gamma\tilde{\gamma}}{\sqrt{(1 + \gamma^2)(1 + \tilde{\gamma}^2)}}} = \sqrt{2 - 2 \sqrt{1 - \frac{(\gamma - \tilde{\gamma})^2}{(1 + \gamma^2)(1 + \tilde{\gamma}^2)}}} \\ & < \sqrt{2 - 2 \sqrt{1 - (\gamma - \tilde{\gamma})^2}} < \sqrt{2} |\gamma - \tilde{\gamma}|. \end{aligned} \quad (4.76)$$

Thus, computing γ to precision $\frac{\epsilon^2}{18}$ ensures an additional error at most $\frac{\epsilon}{3}$. This can be achieved by estimating C with error $n_0^{-\beta} \frac{\epsilon^2}{36}$ and C_1 with error $\frac{\epsilon^2}{36} \frac{C^2}{C_1} > \frac{\epsilon^2}{36} \frac{n_0^{-2\beta}}{n_0} = \frac{\epsilon^2}{36} n_0^{-1-2\beta}$ using Euler-Maclaurin summation with

Poly($\log(1/\varepsilon), \log\left(\frac{1}{|1-\beta|}\right), \beta, \log(n_1), v$) classical computations. Hence, $|\psi_0\rangle_e$ can be prepared with accuracy ε using

$$\text{Poly}(\log(1/\varepsilon), \log(n_1), \log\left(\frac{1}{|1-\beta|}\right), \beta, v) \quad (4.77)$$

gates and ancilla qubits. \square

Theorem 4.11 (Initial state preparation (Methods, Theorem 3)). *Let $\beta > 0$, $\beta \neq 1$ and $N \in \mathbb{N}$. Define*

$$|\psi_0\rangle = \frac{1}{C} \sum_{n=1}^N n^{-\beta/2} |n\rangle, \quad C = \sqrt{\sum_{n=1}^N n^{-\beta}}. \quad (4.78)$$

Then $|\psi_0\rangle$ can be prepared on a quantum computer to precision $\varepsilon > 0$, with success probability at least $(\frac{1}{2} - \frac{\varepsilon}{3})$. The required number of gates and ancilla qubits is bounded by

$$\text{Poly}(\log(1/\varepsilon), \log(N), \log\left(\frac{1}{|1-\beta|}\right), \beta, v), \quad (4.79)$$

where v denotes the number of significant digits used to represent β .

Proof. Set $c = \left\lceil \frac{1}{2} \log_{2\pi} \left(\frac{144}{\varepsilon} \right) \right\rceil$, and choose n_0 so that $(n_0 - 1)$ is the smallest power of 2 larger than $\lceil \beta + 2c \rceil$. Let n_1 be the smallest integer larger than N with $n_1 - n_0$ a power of 2. By Corollary 4.10, the extended state

$$|\psi_0\rangle = \frac{1}{C} \sum_{n=1}^{n_1-1} n^{-\beta/2} |n\rangle \quad (4.80)$$

can be constructed to precision $\frac{\varepsilon}{6}$ using

$$\text{Poly}(\log(1/\varepsilon), \log(n_1), \log\left(\frac{1}{|1-\beta|}\right), \beta, v) = \text{Poly}(\log(1/\varepsilon), \log(N), \log\left(\frac{1}{|1-\beta|}\right), \beta, v) \quad (4.81)$$

gates and ancilla qubits.

Let P denote the projector onto the subspace spanned by $\{|n\rangle : 1 \leq n \leq N\}$, given by:

$$P = \sum_{n=1}^N |n\rangle\langle n|, \quad (4.82)$$

which can be implemented using an ancilla qubit, a comparator, and a measurement. After projection P , the system ideally collapses to the desired state

$$|\psi\rangle = \frac{1}{C} \sum_{n=1}^N n^{-\beta/2} |n\rangle \quad (4.83)$$

with ideal success possibility

$$\frac{\sum_{n=1}^N n^{-\beta}}{\sum_{n=1}^{n_1-1} n^{-\beta}} > \frac{N}{n_1 - 1} \geq \frac{N}{2(N - n_0) + n_0 - 1} \geq \frac{N}{2N - 3} > \frac{1}{2}, \quad (4.84)$$

since $n^{-\beta}$ is positive and decreasing for $\beta > 0$.

In practice, the extended state is prepared to precision $\frac{\varepsilon}{6}$. Let $|\psi_0\rangle$ and $|\widetilde{\psi}_0\rangle_e$ denote the ideal and actual extended state. Then the ideal and actual post-selected states can be written as

$$|\psi_0\rangle = \frac{P|\psi_0\rangle_e}{\sqrt{\langle \psi_0 |_e P | \psi_0 \rangle_e}}, \quad |\widetilde{\psi}_0\rangle = \frac{P|\widetilde{\psi}_0\rangle_e}{\sqrt{\langle \widetilde{\psi}_0 |_e P | \widetilde{\psi}_0 \rangle_e}}. \quad (4.85)$$

The precision in $|\widetilde{\psi}_0\rangle_e$ and the contractive property of P imply that

$$\|\sqrt{\langle \psi_0 |_e P | \psi_0 \rangle_e} |\psi_0\rangle - \sqrt{\langle \widetilde{\psi}_0 |_e P | \widetilde{\psi}_0 \rangle_e} |\widetilde{\psi}_0\rangle\| = \|P|\psi_0\rangle_e - P|\widetilde{\psi}_0\rangle_e\| \leq \| |\psi_0\rangle_e - |\widetilde{\psi}_0\rangle_e \| \leq \frac{\varepsilon}{6}. \quad (4.86)$$

Furthermore, using the triangle inequality

$$|\langle \psi_0 |_e P | \psi_0 \rangle_e - \langle \widetilde{\psi}_0 |_e P | \widetilde{\psi}_0 \rangle_e| \leq |\langle \psi_0 |_e P | \widetilde{\psi}_0 \rangle_e - \langle \widetilde{\psi}_0 |_e P | \widetilde{\psi}_0 \rangle_e| + |\langle \psi_0 |_e P | \psi_0 \rangle_e - \langle \psi_0 |_e P | \widetilde{\psi}_0 \rangle_e| \leq \frac{\varepsilon}{3}. \quad (4.87)$$

Since $\langle \psi_0 |_e P | \psi_0 \rangle_e \geq \frac{1}{2}$, it follows that

$$\left| \sqrt{\langle \psi_0 |_e P | \psi_0 \rangle_e} - \sqrt{\langle \widetilde{\psi}_0 |_e P | \widetilde{\psi}_0 \rangle_e} \right| = \frac{|\langle \psi_0 |_e P | \psi_0 \rangle_e - \langle \widetilde{\psi}_0 |_e P | \widetilde{\psi}_0 \rangle_e|}{\sqrt{\langle \psi_0 |_e P | \psi_0 \rangle_e} + \sqrt{\langle \widetilde{\psi}_0 |_e P | \widetilde{\psi}_0 \rangle_e}} \leq \frac{\sqrt{2\varepsilon}}{3}. \quad (4.88)$$

Using the triangle inequality and combining the Equations (4.86) and (4.88),

$$\begin{aligned} & \left| \sqrt{\langle \psi_0 | eP | \psi_0 \rangle_e} \| |\psi_0\rangle - |\widetilde{\psi}_0\rangle \| - \sqrt{\langle \psi_0 | eP | \psi_0 \rangle_e} \| |\widetilde{\psi}_0\rangle \| \right| \\ & \leq \left| \sqrt{\langle \psi_0 | eP | \psi_0 \rangle_e} - \sqrt{\langle \widetilde{\psi}_0 | eP | \widetilde{\psi}_0 \rangle_e} \right| \| |\widetilde{\psi}_0\rangle \| + \left| \sqrt{\langle \psi_0 | eP | \psi_0 \rangle_e} - \sqrt{\langle \widetilde{\psi}_0 | eP | \widetilde{\psi}_0 \rangle_e} \right| \| |\widetilde{\psi}_0\rangle \| \\ & \leq \frac{\varepsilon}{6} + \frac{\sqrt{2}\varepsilon}{3}. \end{aligned} \quad (4.89)$$

Given $\langle \psi_e | P | \psi_e \rangle \geq \frac{1}{2}$, we have the stated bound

$$\| |\psi_0\rangle - |\widetilde{\psi}_0\rangle \| \leq \frac{1+2\sqrt{2}}{3\sqrt{2}}\varepsilon < \varepsilon, \quad (4.90)$$

and success possibility satisfies

$$\langle \widetilde{\psi}_0 | eP | \widetilde{\psi}_0 \rangle_e \geq \frac{1}{2} - \frac{\varepsilon}{3}. \quad (4.91)$$

Thus, the ideal state $|\psi_0\rangle$ can be prepared with precision ε with at least the success probability as claimed. \square

Supplementary Note 5: Construction of the evolution operator

We now demonstrate the construction of the evolution operator.

Theorem 5.1 (Evolution operator construction (Methods, Theorem 4)). *Define the time evolution operator*

$$U(t) = e^{-iH_0 t}, \quad H_0 = \sum_{n=1}^N \log(n) |n\rangle\langle n|, \quad (5.1)$$

where the evolution time t is specified with u significant digits. Then $U(t)$ can be implemented to precision ξ using

$$\text{Poly}(\log(N), \log(|t|), \log(1/\xi), u) \quad (5.2)$$

gates and ancilla qubits.

Proof. Consider an input state of the form

$$\sum_{n=1}^N \alpha_n |n\rangle |0\rangle, \quad (5.3)$$

where $|0\rangle$ represents the ancilla register. Applying the logarithm oracle L produces

$$\sum_{n=1}^N \alpha_n |n\rangle |\log(n)\rangle. \quad (5.4)$$

Multiplying $\log(n)$ by t yields

$$\sum_{n=1}^N \alpha_n |n\rangle |\log(n)t\rangle. \quad (5.5)$$

Applying controlled R_z rotations results in

$$\sum_{n=1}^N \alpha_n e^{-i\log(n)t} |n\rangle |\log(n)t\rangle. \quad (5.6)$$

Uncomputing the multiplication and applying inverse logarithm oracle L^{-1} leaves

$$\sum_{n=1}^N \alpha_n e^{-i\log(n)t} |n\rangle |0\rangle = U \sum_{n=1}^N \alpha_n |n\rangle |0\rangle. \quad (5.7)$$

In practice, the logarithm $\log(n)$ is approximated by $\widetilde{\log(n)}$ with error at most $\xi/|t|$. This ensures that

$$\left\| \sum_{n=1}^N \alpha_n (e^{-i\widetilde{\log(n)}t} - e^{-i\log(n)t}) |n\rangle \right\| \leq 2 \sin\left(\frac{\xi}{2}\right) < \xi. \quad (5.8)$$

Thus, the distance between the achieved and ideal U is bounded by ξ . By Lemma 3.2, the logarithm oracle and its inverse can be realized using $\log^3(N) \log^2(|t|/\xi)$ gates and $\log^2(N) \log(|t|/\xi)$ ancilla qubits. Multiplying $\log(n)$ by t requires $(\log(|t|/\xi) + \log(N)) u$ gate operations and $(\log(|t|/\xi) + \log(N)) + u$ ancilla qubits. The controlled R_z gates

can be implemented qubit by qubit with $\mathcal{O}(\log(N) + \log(|t|/\xi))$ gates. Combining these bounds, the total resource requirement for implementing $U(t)$ is

$$\text{Poly}(\log(N), \log(|t|), \log(1/\xi), u) \quad (5.9)$$

gates and ancilla qubits, completing the proof. \square

Supplementary Note 6: Upper bound of $\zeta'(s)$ for $0 < \beta < 1$

We establish upper bounds for the Dirichlet eta function $\eta(s)$ and its derivative $\eta'(s)$, defined as

$$\eta(s) = \sum_{n=1}^{\infty} (-1)^{n+1} n^{-s}, \quad \eta'(s) = - \sum_{n=1}^{\infty} (-1)^{n+1} \ln n n^{-s}. \quad (6.1)$$

Then $\eta(s)$ can be expressed as:

$$\eta(s) = \sum_{n=1}^{\infty} (-1)^{n+1} n^{-s} = \sum_{n=1}^{\infty} ((2n-1)^{-s} - (2n)^{-s}) = \sum_{n=1}^{\infty} s \int_{2n-1}^{2n} \nu^{-s-1} d\nu. \quad (6.2)$$

Taking the absolute value, we obtain

$$|\eta(s)| \leq |s| \sum_{n=1}^{\infty} \int_{2n-1}^{2n} \nu^{-\beta-1} d\nu < |s| \int_1^{\infty} \nu^{-\beta-1} d\nu = \frac{|s|}{\beta}. \quad (6.3)$$

Similarly, for the derivative $\eta'(s)$, we have

$$\eta'(s) = - \sum_{n=1}^{\infty} (-1)^{n+1} (\ln n) n^{-s} = \sum_{n=1}^{\infty} (\ln(2n)(2n)^{-s} - \ln(2n-1)(2n-1)^{-s}) = \sum_{n=1}^{\infty} \int_{2n-1}^{2n} (-s\nu^{-s-1} \ln \nu + \nu^{-s-1}) d\nu. \quad (6.4)$$

Hence,

$$|\eta'(s)| \leq |s| \int_1^{\infty} |\nu^{-s-1}| \ln \nu d\nu + \int_1^{\infty} |\nu^{-s-1}| d\nu = |s| \int_1^{\infty} \nu^{-\beta-1} \ln \nu d\nu + \int_1^{\infty} \nu^{-\beta-1} d\nu = \frac{|s|}{\beta^2} + \frac{1}{\beta}. \quad (6.5)$$

Since the zeta function is related to $\eta(s)$ by

$$\zeta(s) = \frac{1}{1-2^{1-s}} \sum_{n=1}^{\infty} \frac{(-1)^{n+1}}{n^s} = \frac{1}{1-2^{1-s}} \eta(s). \quad (6.6)$$

Its derivative $\zeta'(s)$ is:

$$\zeta'(s) = \frac{d}{ds} \left(\frac{1}{1-2^{1-s}} \sum_{n=1}^{\infty} \frac{(-1)^{n+1}}{n^s} \right) = \frac{\eta'(s)(1-2^{1-s}) - 2^{1-s} \ln 2 \eta(s)}{(1-2^{1-s})^2}. \quad (6.7)$$

Using the previously established bounds

$$|\eta(s)| \leq \frac{|s|}{\beta}, \quad |\eta'(s)| \leq \frac{|s|}{\beta^2} + \frac{1}{\beta},$$

we obtain the bound for $\zeta'(s)$:

$$|\zeta'(s)| \leq \frac{|s|}{|2^{1-\beta} - 1|\beta} + \frac{2^{1-\beta} \ln 2 (|s|\beta + 1)}{|2^{1-\beta} - 1|^2 \beta^2} = \mathcal{O}\left(\frac{|s|}{\beta|1-\beta|} + \frac{|s|\beta + 1}{|1-\beta|^2 \beta^2}\right) = \text{Poly}(|t|, |1-\beta|^{-1}, \beta^{-1}), \quad (6.8)$$

given that $|2^{1-\beta} - 1| \geq \ln(2)|1-\beta|$ for all $0 < \beta < 1$.

Supplementary Note 7: Order of $|\chi(s)|$ for $0 < \beta < 1$

Recall that

$$\chi(s) = 2^s \pi^{s-1} \sin\left(\frac{\pi s}{2}\right) \Gamma(1-s). \quad (7.1)$$

Thus,

$$|\chi(s)| = 2^\beta \pi^{\beta-1} \left| \sin \frac{\pi s}{2} \right| |\Gamma(1-s)|. \quad (7.2)$$

We focus on $s = \beta + it$ with $0 < \beta < 1$,

$$\sin\left(\frac{\pi s}{2}\right) = \sin\left(\frac{\pi\beta}{2} + \frac{i\pi t}{2}\right) = \sin\left(\frac{\pi\beta}{2}\right) \cosh\left(\frac{\pi t}{2}\right) + i \cos\left(\frac{\pi\beta}{2}\right) \sinh\left(\frac{\pi t}{2}\right), \quad (7.3)$$

so we obtain

$$|\sin(\pi s)| = \sqrt{\sin^2\left(\frac{\pi\beta}{2}\right) \cosh^2\left(\frac{\pi t}{2}\right) + \cos^2\left(\frac{\pi\beta}{2}\right) \sinh^2\left(\frac{\pi t}{2}\right)} = \sqrt{\sinh^2\left(\frac{\pi t}{2}\right) + \sin^2\left(\frac{\pi\beta}{2}\right)} = \Theta(e^{\pi|t|/2}). \quad (7.4)$$

Using Stirling's formula in the sector $|\arg z| \leq \pi - \varepsilon$,

$$\Gamma(z) = \sqrt{2\pi} z^{z-\frac{1}{2}} e^{-z} (1 + O(|z|^{-1})). \quad (7.5)$$

Taking absolute values gives

$$|\Gamma(z)| = \sqrt{2\pi} |z|^{z-\frac{1}{2}} e^{-\operatorname{Re}(z)} (1 + O(|z|^{-1})). \quad (7.6)$$

Note that

$$|z^{z-\frac{1}{2}}| = \exp(\operatorname{Re}(\ln(z)(z - \frac{1}{2}))) = \exp(\ln(|z|)(\operatorname{Re}(z) - \frac{1}{2}) - \arg(z) \operatorname{Im}(z)) = |z|^{\operatorname{Re}(z) - \frac{1}{2}} e^{-\arg(z) \operatorname{Im}(z)}. \quad (7.7)$$

Now we set $z = 1 - s = (1 - \beta) - it$, then

$$|\Gamma(1 - s)| = \sqrt{2\pi} |1 - s|^{1/2-\beta} e^{t \arg(z)} e^{-(1-\beta)} (1 + O(|t|^{-1})). \quad (7.8)$$

For $t < 0$, $\arg z = \arctan\left(\frac{|t|}{1-\beta}\right)$, so

$$\exp(t \arg z) = \exp\left(t \operatorname{arccot} \frac{1-\beta}{|t|}\right) = \exp\left(t\left(\frac{\pi}{2} - \frac{1-\beta}{|t|} + \mathcal{O}(|t|^{-3})\right)\right) = \exp(-\pi|t|/2) \exp((1-\beta))(1 + \mathcal{O}(|t|^{-2})). \quad (7.9)$$

For $t > 0$, $\arg(z) = -\arctan\left(\frac{t}{1-\beta}\right)$, so

$$\exp(t \arg(z)) = \exp\left(-t \operatorname{arccot} \frac{1-\beta}{t}\right) = \exp\left((-t)\left(\frac{\pi}{2} - \frac{1-\beta}{t} + \mathcal{O}(|t|^{-3})\right)\right) = \exp(-\pi t/2) \exp((1-\beta))(1 + \mathcal{O}(t^{-2})). \quad (7.10)$$

In both cases,

$$\exp(t \arg z) = \exp(-\pi|t|/2) \exp((1-\beta))(1 + \mathcal{O}(|t|^{-2})). \quad (7.11)$$

Therefore,

$$|\Gamma(1 - s)| = \sqrt{2\pi} |1 - s|^{1/2-\beta} \exp(-\pi|t|/2) (1 + \mathcal{O}(|t|^{-1})). \quad (7.12)$$

Combining terms,

$$|\chi(s)| = \Theta(1) 2^\beta \pi^{\beta-1} \exp(\pi|t|/2) \sqrt{2\pi} |1 - s|^{1/2-\beta} \exp(-\pi|t|/2) (1 + \mathcal{O}(|t|^{-1})), \quad (7.13)$$

The exponential terms cancel, leaving

$$|\chi(s)| = \Theta(|1 - s|^{1/2-\beta}) = \Theta(|t|^{1/2-\beta}). \quad (7.14)$$